Master's Thesis

Methylation-Dependent DNA Condensation : Its Implications in Chromosome Organization and Epigenetic Gene Control.

Hyunju Kang

Department of Biomedical Engineering

Graduate School of UNIST

2017

Methylation-Dependent DNA Condensation
: Its Implications in Chromosome Organization and Epigenetic Gene Control.

Hyunju Kang

Department of Biomedical Engineering

Graduate School of UNIST

Methylation-Dependent DNA Condensation : Its Implications in Chromosome Organization and Epigenetic Gene Control.

A thesis/dissertation
submitted to the Graduate School of UNIST
in partial fulfillment of the
requirements for the degree of
Master of Science

Hyunju Kang

01. 06. 2017 of submission

Approved by

Advisor
Hajin Kim

Methylation-Dependent DNA Condensation : Its Implications in Chromosome Organization and Epigenetic Gene Control.

Hyunju Kang

This certifies that the thesis of Hyunju Kang is approved.

01.06. 2017 of submission

signature

Advisor: Hajin Kim

signature

typed name: Taejoon Kwon

signature

typed name: Jung-Min Kee

Abstract

The methylation of CpG sites on genome has been known to play a crucial role in epigenetic gene regulation. We hypothesize that the C5 methyl group modulates the attractive interaction between double stranded DNAs in the presence of biogenic polyamines like spermine and poly-lysine. We designed a set of experiments with sequence-controlled and chemically modified DNAs to test the hypothesis. We made dsDNAs that have TA-rich, CG-rich, CpG-methylated (mCG) - rich, or UA-rich sequence and measured their propensity to form aggregates by precipitation and ensemble FRET measurements. In the presence of spermine, TA-rich or mCG-rich dsDNAs, both having the C5methyl group on T or mC, exhibited significantly stronger affinity than CG-rich or UA-rich ones that do not contain the methyl group. Similar trend was observed in the presence of hexa-lysine, which models the lysine-rich histone tails. These results suggest the critical role of the additional methyl group in determining the attractive potential between dsDNAs. From multi-color single molecule FRET measurements on vesicle-encapsulated pairs of dsDNAs, we found that the DNA binding dynamics is temporally anti-correlated with the DNA bending dynamics, consistent with the methylation-dependent DNA looping previously observed. From all-atom molecular dynamics simulations, we propose the physical mechanism for the methylation-dependent attraction based on the steric repulsion of polyamines by the C5 methyl group. Our findings suggest plausible explanations for the physical origin of the chromosome arrangement and its epigenetic modulation.

Contents

List of Figure

List of Table

.

Introduction

The spatio-temporal organization of the chromosomes plays a key role in regulating gene expression and maintaining genomic stability [1-4]. The control of physical interaction between dsDNAs comprises an essential part of this. In addition to the protein-mediated, programmed structuring of the chromatins, direct electrostatic interaction between dsDNAs can be a crucial factor if it varies upon the DNA sequence or chemical modifications such as cytosine methylation. dsDNAs are basically repulsive to one another being negatively charged, but they can turn attractive in the presence of polycations resulting in strong condensation, as revealed over a long history [5-11]. In our recent study, we presented evidences that the C5 methyl group present in thymine or methylated cytosine augments the condensation power of a biogenic polyamine, spermine, suggesting a possible mechanism for non-Watson crick sequence recognition between dsDNAs [12].

In this work, we quantified the polyamine-driven condensation of sequence-controlled and chemically modified DNAs by ensemble FRET and precipitation measurement. We used two types of polyamines: poly-lysine and spermine. Poly-lysine was used as a simplifying mimic for the lysine-rich histone tail. Both types of polyamines exhibited a tendency to condense thymine-rich (TA-rich) DNAs at lower concentration than cytosine-rich (CG-rich) ones and the contrast became larger when the sequence was arranged to have more consecutive thymines or cytosines. Such tendency was cross-confirmed to be due to the C5 methyl group as its addition to the CG-rich (mCG-rich) DNAs resulted in stronger condensation while its subtraction from the TA-rich (UA-rich) DNAs resulted in weaker condensation. From MD simulations, we found this is due to the steric repulsion of the polyamine chains out of the DNA grooves by the hydrophobic methyl groups, positioning them at the bridging sites between the dsDNAs. Flexibility of the dsDNAs is another factor to determine the nuclear architecture of the chromatins and it has also been found to depend on the methylation pattern [13-15]. Interestingly, from three-color single molecule FRET (smFRET) measurements we found that the bending dynamics negatively correlates with the binding dynamics between a single pair of dsDNAs.

From this study, we prove methylation content governs DNA condensation through steric repulsion against biogenic polyamines, and found their anti-correlated physical dynamics with dsDNA looping. .Implication from the physical origin of the modulated dsDNA properties in our finding will be discussed

1.1 Chromosome organization

This research is started from epigenetic regulation. Epigenetics is the study that focus on changes in gene expression such as active or inactive genes which does not related with changes to DNA sequence. Epigenetic change is a regular and natural phenomena, and It is well known that chromosome organization is important role in epigenetic regulation.[16, 17]

Chromosome organization happen from movement of chromatin from a condensed formation to a transcriptionally open formation. This mobility enable to be accessible or inaccessible DNA from transcription factors or other DNA binding proteins, and regulate gene expressionDNA methylation, histone modification are also well known to highly related with this chromatin organization. [17] New and ongoing studies are continuously uncovering the role of DNA and histone modifications in chromosome organization, and their implication in epigenetic gene control. Especially methylation on DNA or histone is well known that change the structure of chromosome from transcription factors mediated reaction.[16, 18, 19] For example, One of previous research about X chromosome imaging provided that hyper- methylated X chromosome is genetically inactive and appears more compact than this active counterpart, it presented function of methylation which affect the chromosome compaction and genetic inactivation[20] In the same line, recent study also presented that noncoding AT rich DNA region acts as architectural roles for dynamic regulation of the epigenetic gene control. Comparing to GC rich DNA, AT rich DNA has methyl-group on 5 carbon of thymine ring, it suggest methyl-group which related histone methylation and DNA methylation plays key role in chromosome compaction on chromosome organization. [21] However specific mechanism and the driving force behind the chromosome organization with methylation on histone and DNA are still not discovered. In this study, we focus on the histone and DNA methylation which are well known to important role in chromosome organization, and aim to uncover the physical mechanism of DNA dynamics from histone modification and DNA methylation for chromosome organization mechanism

1.1.1 Histone modification

A histone modification is a covalent post-translational modification (PTM) to histone proteins which includes methylation, acetylation, phosphorylation etc. The PTMs from histones can affect gene regulation by altering chromatin structure such as closed chromatin or open chromatin.[22, 23] Usually, it is well known that histone H3 and H4 primarily acetylated or methylated at positive charged lysine residues play important role chromosome organization mediated transcription factors.[24] Therefore,

The comparison of various histone function and observation of their modifications would provide helpful information about epigenetic regulation on chromosome [12, 25], Because histone forms the beads and string formation with DNA, DNA flexibility and condensation on histone are considered to important role in organize chromosome.[26] Based on these reason, this research used hexa-lysine (6lysine) as analogue of histone and aimed to uncover the physical mechanism behind epigenetic regulation from interaction between positive charged lysine residues and DNA. Furthermore, by using modified lysine such as tri-methylated lysine, we intended to discover the model histone modification effect on the DNA condensation compare to unmodified model histone 6lysine.

1.1.2 DNA methylation

DNA methylation is another epigenetic modification that occurs by the addition of a methyl group to 5-caborn of DNA, thereby often regulating the function of the genes. In many case, DNA methylation process is the covalent addition of the methyl group at the 5-carbon of the cytosine ring resulting in 5-methylcytosine (5-mC). These methyl groups project into the major groove of DNA and inhibit transcription with enzyme mediated interactions.[27] The addition of methyl groups on DNA is controlled by a family of DNA methyltransferases (DNMTs) which establish and maintain DNA methylation patterns.[24] DNA demethylation, the removal of a methyl group, is also well known that involved in many important Epigenetic regulation. [28] However, specific role of methylation still not discovered.

Recent studies presented sequence-dependent attraction is controlled by methylation and its pattern.[12], in this study also focus on the AT rich DNA compare to GC rich DNA with methyl group, they found that AT rich DNA has same tendency of dsDNA-dsDNA attraction with methylated Cytosine rich DNA.[12] DNA flexibility is also governed by DNA methylation, not other 5-mC modifications. [29] These studies commonly focused on 5-mC on DNA sequence as alternate view of epigenetic control of chromosome. From this studies, we can hypothesize that there is some correlation between DNA condensation and flexibility governed by C5 DNA methylation.

Thanks to the development of single molecule FRET measurement technique, we can measure not only single event between biomolecule samples but also multiple dynamics among dsDNA molecules such as dsDNA bending and binding at the same time. From this multi-color single molecule technique, we ultimately aim to measure the multiple dynamics between a pair of dsDNA according to DNA methylation with polyamine to uncover fundamental mechanism of the chromosome organization.

1.2 FRET

A variety of biological events happen in nanometer scale. However conventional optical microscopy does not work in this nanometer scale range, to overcome this visualizing limitation, diverse micro-techniques have been developed. One of this is Fluorescence resonance energy transfer (FRET) measurement, it provided information about inter molecular interaction. After single molecule FRET technique have been developed, complicated dynamics and mobility of biological molecules have predicted.

The first observation of FRET phenomenon was recorded in 1922. Cario and Franck found that energy transfer from mercury to thallium. [30] Based on this observation, specific FRET mechanism discovered as electrodynamic interaction such as dipole-dipole interaction[31], and then FRET efficiency: E was calculated as a function of the distance between the donor and the acceptor.[32] (Equation 1.1)

$$E = \frac{1}{1+\frac{R^6}{R_0{}^6}} \qquad \text{(Equation 1.1)}$$

In this FRET efficiency equation , where R represent the distance between the two fluorophore molecules, and R_0 represents a characteristic distance such as 50% of FRET efficiency from properties of the fluorophores and environmental factors. This equation experimentally conformed after 1960's and was computed below graph. (Figure 1.1)

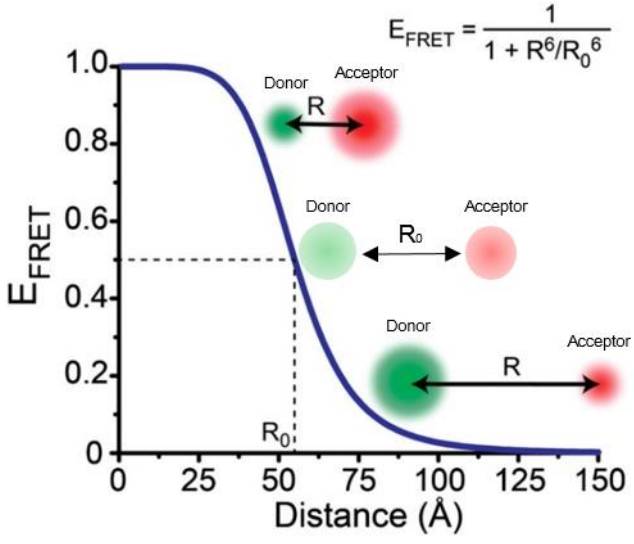

Figure 1.1. A graph of FRET efficiency following distance(R) between a donor and acceptor fluorophore molecules [33]. This plot can be shifted according to properties of fluorophores and environmental factors

Because FRET efficiency is the efficiency of fluorescent energy transfer, the raw intensity of a Donor-Acceptor pair can be used experimentally for calculating FRET efficiency. There are many number of way measuring energy transfer from the intensity of donor and accepter. Usually donor emission intensity and donor/accepter intensity ratio are used for calculating FRET efficiency.

1.2.1 FRET efficiency from donor emission

If the absorbance of donor at the excitation wavelength is identical between two samples in the property such as the excitation wavelengths and concentrations, two emission intensity according to the wavelength are used for the FRET intensity calculation; *E* can be calculated as (Equation 1.2)

$$E = 1 - \frac{I_{DA}}{I_D} \quad \text{(Equation 1.2)}$$

Where I_{DA} is the total donor fluorescence intensities in presence and I_D is the total donor fluorescence in absence of acceptor. This calculation provides absolute value according to the difference of quantum yield between donor and acceptor. However it is hard to get exact same concentration from experimental samples, this method need for adjustment to make same experimental condition. So below calculation is used for FRET intensity calculation.

$$E = 1 - \frac{A_D}{A_{DA}} \frac{I_{DA}}{I_D} \quad \text{(Equation 1.3)}$$

Where A_D and A_{DA} are the donor absorbance at the excitation wavelength in the donor only and Donor including acceptor samples, respectively.

1.2.2 FRET efficiency from donor/acceptor intensity ratio

If acceptor is fluorophore which is similar with donor, FRET efficiency is easily calculated using the ratio between the donor and acceptor emission intensities. Because the ratio between the donor and accepter intensities rely on also the fluorescence quantum yields of the two fluorophores, FRET using ratio between the donor and acceptor is a relative value of energy transfer.
This ratiometric FRET value can be calculated like below. (Equation 1.4)

$$E = \frac{I_A}{I_D + I_A} \quad \text{(Equation 1.4)}$$

Where I_A and I_D are the total acceptor and donor fluorescence intensities, respectively, following donor excitation. For this calculation, two correction factors are needed; the contribution from direct acceptor excitation to I_A and the ratio between the each fluorophore quantum yields. The leakage of donor emission into the value of I_A and leakage of acceptor emission into the value of I_D from overlapping the mixed donor & acceptor spectrum also have to adjust in this calculation.

1.3 Single molecule FRET

After 1980's, technical advances such as oxygen-scavenger system and imaging system facilitated to detect single molecule absorption and fluorescence. In 1996, Ha et al suggested the FRET study could be performed at single molecule level[34]. After that, development from CCD camera to EMCCD camera, diverse ways to increase the surface passivation, and stable fluorophore in the single molecule FRET technique enable to apply in various biological studies. [35]

However, It had limitation to explain the various and complicated dynamics at the same time. Because previous 1- dimensional FRET measurement between just two molecules of donor and acceptor could not measure multiple distances, the biological events usually related with multi component interaction could not observe and detect the internal degree of freedom with external interaction. To overcome this problem, multi-color FRET was developed to measure simultaneous events. From this technique, we can measure the correlated motion of multiple biomolecular domains.

1.3.1 Multi-color FRET

To apply multi-color single molecule FRET measurement in biological studies, It is important to select fluorescent dye molecules. There had been attempts at using Cy3, Cy5, Cy5.5 dye trio [35] or Alexa488, TMP, and Cy5 dye trio. [36] However, they have a limitation that could not enough to determine three inter fluorophore distances because of photo-bleaching and huge spectral overlap.[37] These days, as an alternative dye trio: Cy3, Cy5, Cy7 are used for three color FRET technique. They dramatically enable to elongate the total observation time from photo stability and proper spectral overlap.(Figure1.2.)

Based on the Cy3-Cy5-Cy7 dye trio, 3 color FRET technique is expected to provide correct information of multi-domain configurations and their correlated motion using alternating green laser and red laser excitation (ALEX) technique in total internal reflection fluorescence (TIRF) microscopy[37]

By using Cy3-Cy5-Cy7 trio and ALEX technique with green-red laser, we can observe three FRET interactions, E12: FRET from the Cy3 to the Cy5 form green laser, E13: FRET from Cy3 to the Cy7 from green laser, and E23: FRET from the Cy5 to the Cy7 from red laser. From this observation, three fluorescence signals are enough to uniquely determine the two unknown variables, E12 and E13.[35, 38] (Figure1.3)

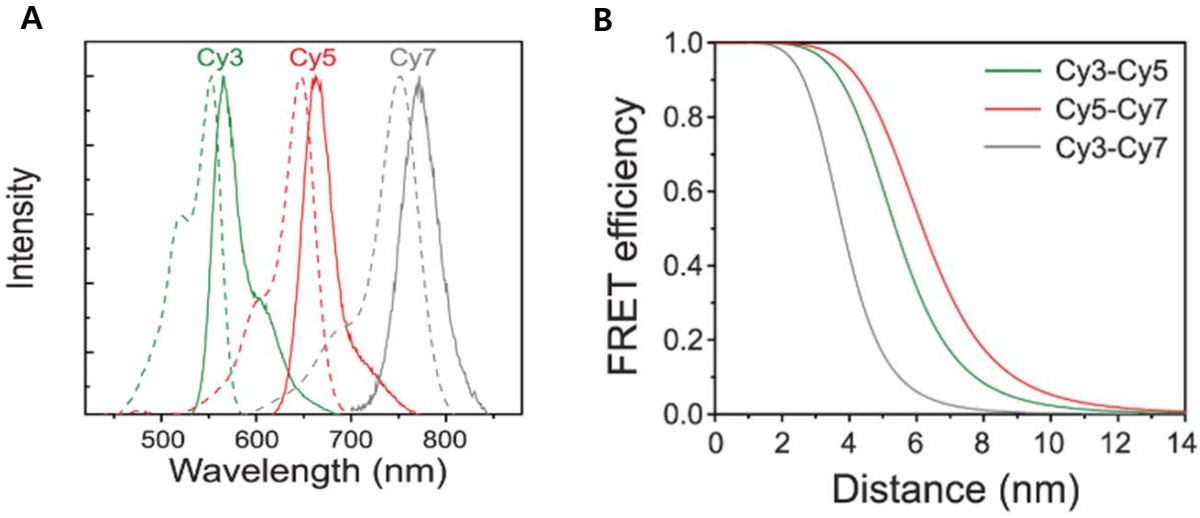

Figure 1.2. Property of Cy3-Cy5-Cy7 trio (A) Solid lines and dash lines represent emission and absorption spectra of Cy3 (green), Cy5 (red) and Cy7 (gray) representatively. (B) FRET efficiencies can be estimated from distance between the each FRET pairs such as Cy3-Cy5 (green), Cy5-Cy7 (red) and Cy3-Cy7 (gray) pairs.[37]

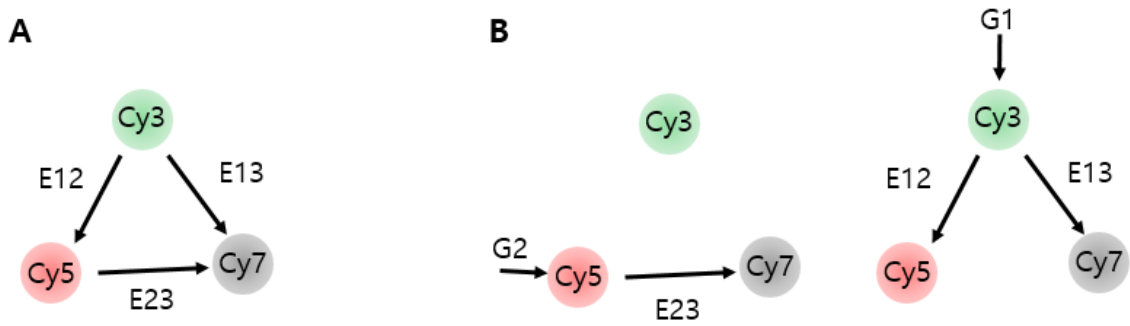

Figure 1.3. A schematic diagrams for determination of 3color FRET efficiencies using the single molecule ALEX technique. (a) FRET interactions between Cy3-Cy5 or Cy3-Cy7 or Cy5-Cy7 from each energy transfer (b) The ALEX technique enable to determine three FRET efficiencies at the same time.[38]

1.3.2 Experimental Setup of TIRF microscopy

There are two way of TIRF microscopy, one is prism type, the other is objective type. We used prism type for our study. The TIRF microscopy setup can be divided into 3 parts, laser excitation path (green box), objective part (red box), emission channel part (blue box). Excited fluorophores are collected to objective and then pass a low pass filter and dichroic mirror to split into donor and acceptor signal. Then final image on EMCCD is imaged side by side and we can match same molecule from each half image and measure the raw intensity of donor and an acceptor molecule to find out FRET efficiency and get the information such as distance between donor and acceptor.

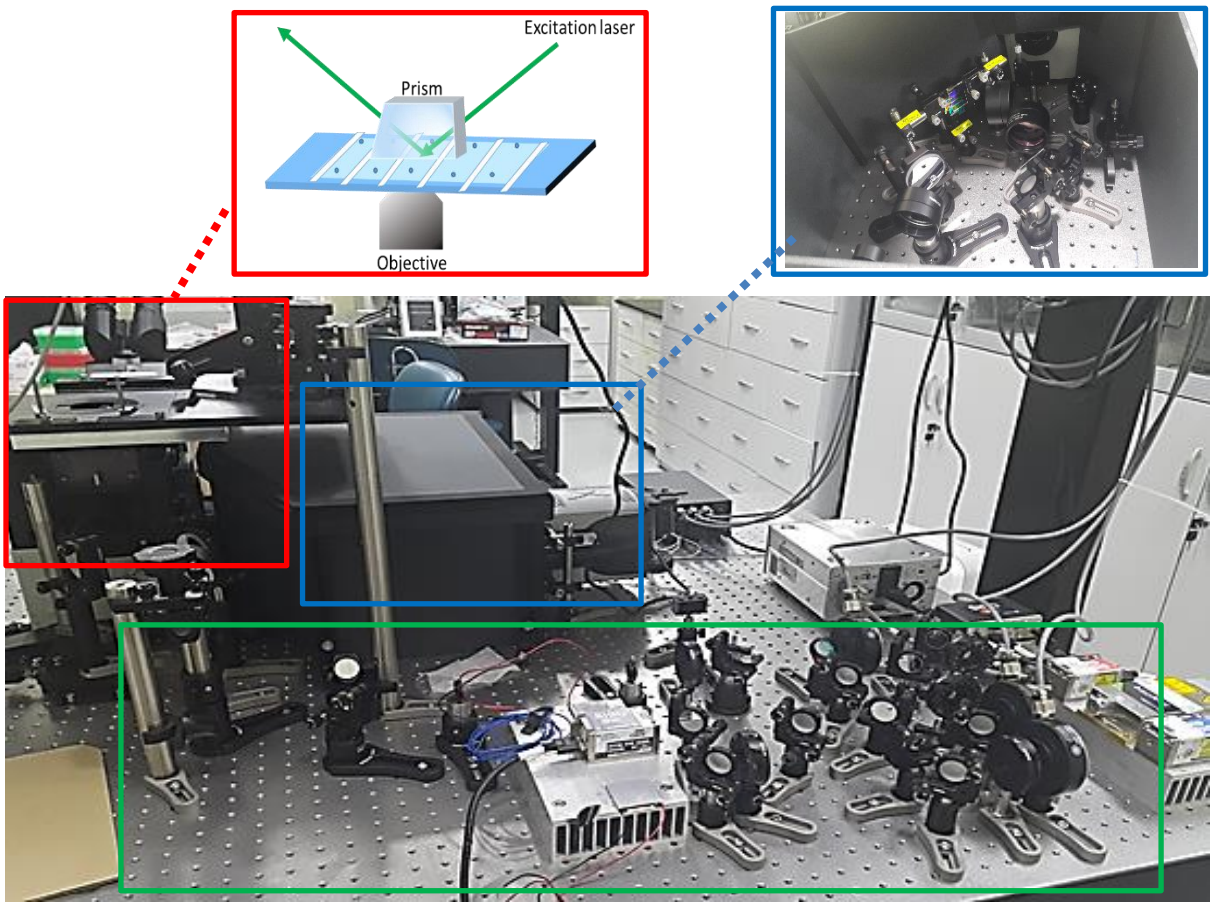

Figure 1.4. TIRF microscopy set up for this experiment. Green Box: Red laser or green laser pass through laser path by reflecting mirrors, ultimately, they are collected to prism to measure donor and acceptor signals. Red Box: We can measure exited fluorophores using prism and objective. The upper red box represent the example of prism type measurement of TIRF microscopy. Blue Box: exited fluorophores provide the information about interaction between samples as raw emission intensity. From the emission channel part, we can detect the signals and calculated FRET efficiency. The upper blue box show the inside of emission channel box.

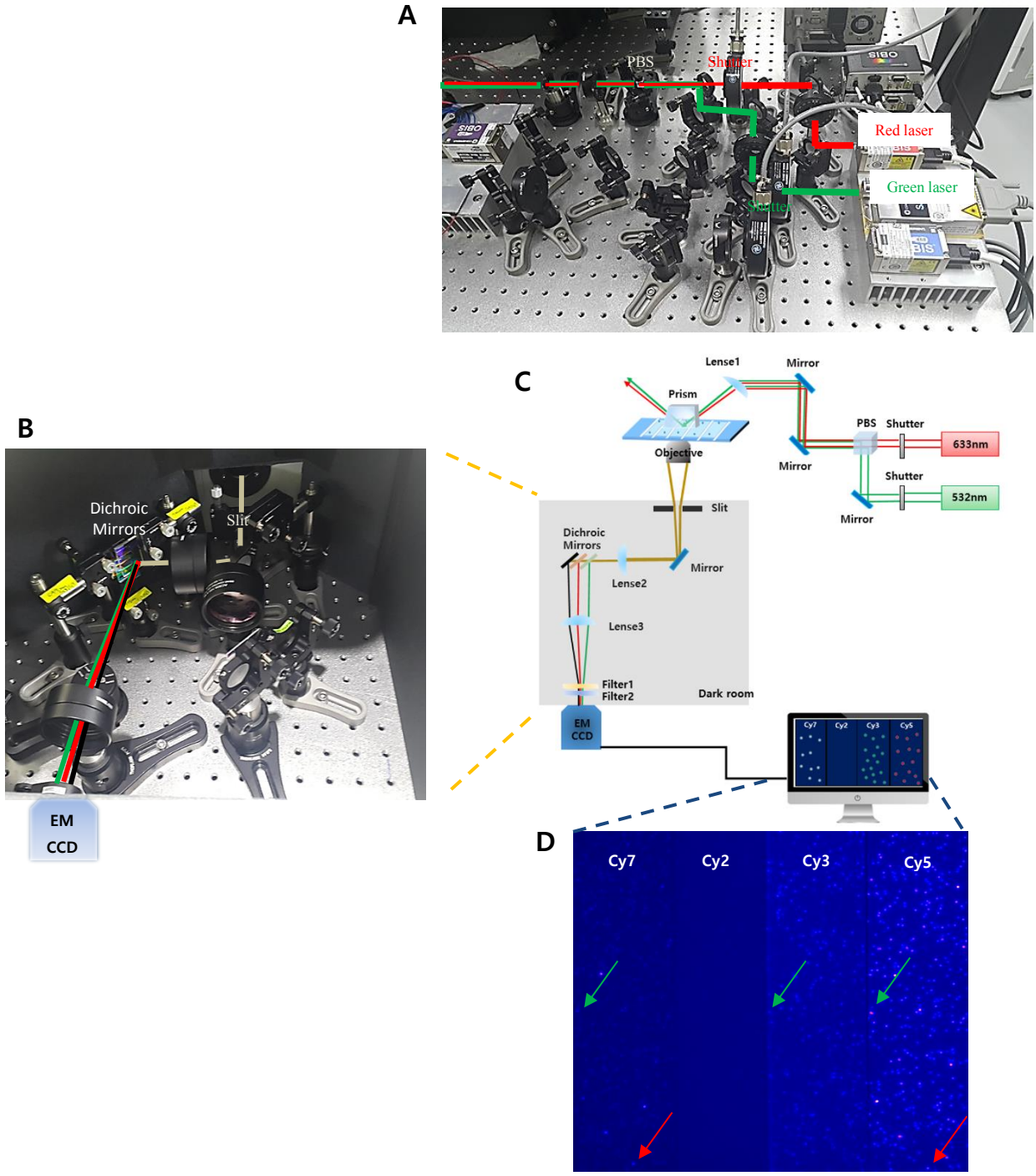

Figure 1.5. TIRF microscopy set up with schematic diagram. (A) Laser excitation path (B) Emission channel part, each dichroic mirror selectively pass light from each range of colors. (C) Schematic diagram of 3color single molecule FRET measurement using TIRF microscopy, PBS(polarizing beam splitter) [37] (D) The output of our measurement. We can predict that there is 2 step energy transfer from spots on Cy3, Cy5, Cy7 channel (green arrow), and 1step energy transfer from spots on Cy5, Cy7 channel (red arrow).

Ⅱ. Materials and Experimental Method

2.1 Materials and Sample Design

2.1.1 DNA Design

In This study, 120bp labeled dsDNA and 120bp non-labeled dsDNA were used for FRET (Ensemble FRET, smFRET) and DNA precipitation measurement respectively. They are properly designed to avoid intramolecular toroid form. [12, 39, 40] we used Cyanine dye, Cy3, Cy5, Cy7 as fluorophore to label each DNA sample

Labeled dsDNAs were made by PCR, in case ensemble FRET measurement, 20bp C6-amine forward primer and 20bp normal reverse primer were used to label Cy3 or Cy5 each one end of DNA,(Figure2.1 A), while we used 20bp C6amine reverse primer for Cy7 labeling with 20bp Cy5 forward primer to measure bending events using multi-color single molecule FRET measurement.(Figure2.1. B) In the DNA precipitation, Non-labeled DNAs were made by 20bp normal primers to prevent hydrophobic influences during DNA precipitation reaction.(Figure2.1. C)

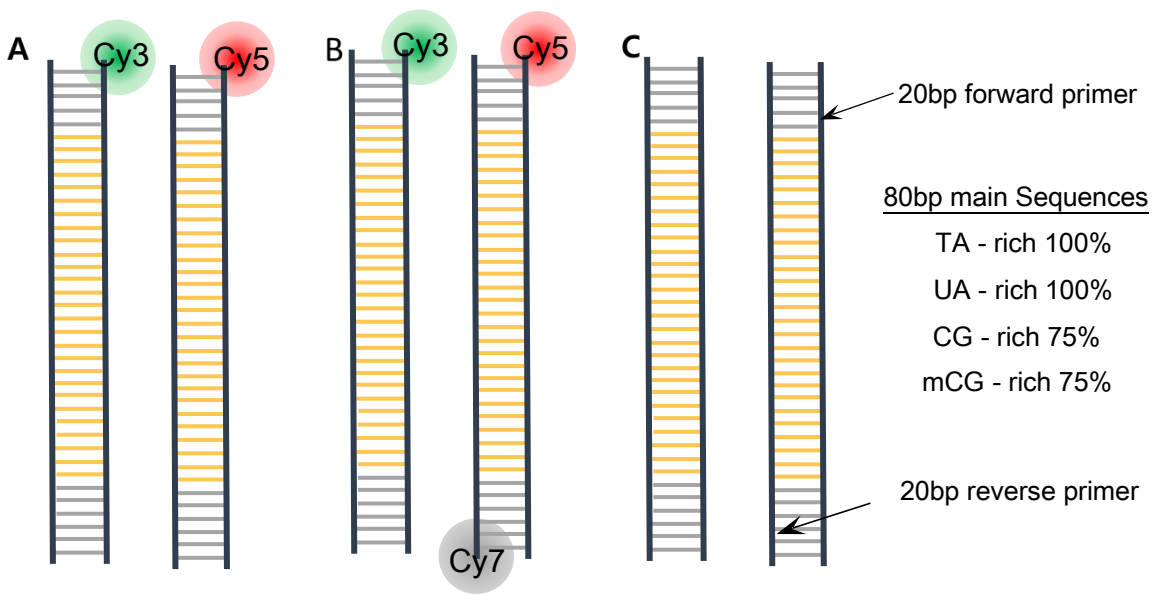

Figure 2.1. Schemetic design of DNA molecules. (A) Labeled DNA for enmsemble FRET, Cy3 or Cy5 is labeled on each one end of dsDNA (B) labeld DNA for multi-color single molecule FRET measurment, In the multi-color single molecule FRET measurment, we added Cy7 flouorophore to measure bending event with Cy5 (C) Non-labeled DNA for DNA precipitation.

We designed 80bp sequence-controlled regions in the middle with common 20-bp primer regions at both ends: 100% TA(TA rich), 25% TA(CG rich), then, in order to dissect the role of the C5 methyl group, we synthesized CG-rich DNAs with methylated Cytosines(mCG-rich) and TA-rich DNAs with thymines replaced by deoxyuridines (UA-rich) (Figure2.2.)

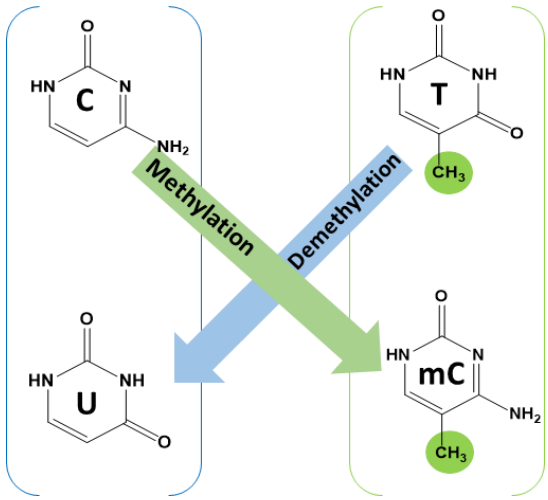

Figure 2.2. Methyl group dependent each DNA base used for 80bp main seuqence design. TA rich and mCG rich DNA have the C5 methyl gorup on Tyimine and methylated Cytosine respectively, while CG rich and UA rich DNA don't have methyl group on C5 of Cytosine and Urasil

The methyl group dependent 120bp of DNA oligos were synthesized by Integrated DNA Technologies (US) with HPLC purification. The methyl group dependent dsDNA constructs produced by PCR using designed 120bp of templates and forward and reverse primers. We used Phusion High-Fidelity PCR Master Mix kit (New England BioLabs) for PCR according to the standard protocol of the kit. The PCR constructs were purified using the PCR purification kit (Jenet bio) and their concentrations were measured by nanodrop using uv-vis absorpsion.

The design of the methylation dependent 120 bp DNA templates are presented in Table 1. Unlike 120bp of TA, CG, mCG rich DNA were made by PCR, UA rich DNA were custom-synthesized by exchanging uracil instead of thymine in only main sequence of TA rich DNA. From this, sense and antisense template of UA DNA are prepared, completed double strand UA rich DNAs were obtained by annealing sense and antisense template at a molar ratio of 1: 1.2 in the annealing buffer (10mM tris-HCl, 1mM EDTA, pH8.0, 50mM NaCl) for final concentration 2uM. An annealing process was conducted by heating at 95C for 5min and slowly cooling down to 25C. The annealing products were purified using the PCR purification kit (Jenet bio) to make same final condition with other dsDNAs. The mCG-rich DNA constructs were obtained by 4 hours methylation reaction using the CpG methyltransferase M. SssI (New England BioLabs, M0226L), according to standard protocol from the company. After the CGCG sites on mCG rich dsDNA were methylated during 4hours incubation, the

constructs were purified by the PCR purification kit (Jenet bio). The methylation efficiency was measured by BstUI restriction enzyme (New England BioLabs, R0518L) which can cut only un-methylated CGCG sequence. After then we performed electrophoresis of the digested fragments using a polyacrylamide gel (Biorad 15%TBE urea gel), we could check the methylated product 120bp site on the gel. [12](Figure 2.3)

In order to present a variety of views about methyl group effect on dsDNA attraction, we observed whether methyl group pattern effect on the attraction between dsDNAs, We designed 100% TA with more consecutive thymines (TTT), 25% TA (CG-rich), 25% TA with more consecutive cytosines (CCC). We obtained TTT dsDNA from PCR like previous method. However, in case CCC dsDNA template, i-motif and G-quadruplex [41, 42] formation inhibit to make full length CCC dsDNA . From this reason, we prepared customized sense and anti-sense template of CCC sequence and obtained dsDNA by annealing like UA rich dsDNA.

Furthermore, we designed additional 60bp, 80bp, 100bp TA rich DNA by reducing thymine number in main sequence to measure length dependent dsDNA attraction. 80bp and 100bp dsDNAs are produced from each templates and two primers by PCR as described earlier. Because 60bp was not compatible with Phusion High-Fidelity PCR master Mix kit, we used another PCR master mix kit (prime taq premix, Jenet bio) for 60bp dsDNA, following the standard protocol of the kit. All DNA products checked through a poly acrylamide gel.(Figure 2.3. B)

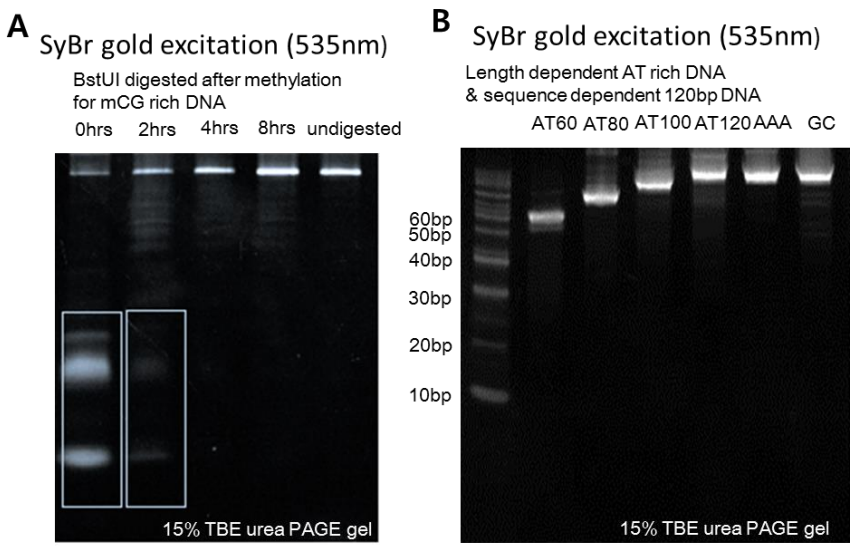

Figure 2.3. Poly acrylamide gel image. (A) Methylation efficiency check for mCG rich DNA, (B) Length dependent DNA products from PCR

Name	Sequence	Ratio				
		A	T	G	C	dU
primer A	5'AGCGGTGATGCTGATAGAAG-3'	6	4	8	2	
primer A (3color FRET)	5'C6 amine AGCGGTGATGCTGATAGAAG-3'	6	4	8	2	
primer B (FRET)	5'C6 amine GGCGCACAGAAGCTATTATG-3'	6	4	6	4	
primer B (precipitation)	5'GGCGCACAGAAGCTATTATG-3'	6	4	6	4	
TA TA rich DNA	5'AGCGGTGATGCTGATAGAAGTATAATATTAATAATAAATTAAATATATTATATTAATAATTAATAATTAATAAATTAAAATATTATTTATAATAATTAAACATAATAGCTTCTGTGCGCC-3'	55	45	12	8	
UA1 UA-rich DNA Sense	5'AGCGGTGATGCTGATAGAAGUAUAAUAUUAAUAAUAAAUUAAAUAUAUUAUAUUAAUAAUUAAUAAUUAAUAAAUUAAAAUAUUAUUUUAUAAUAAUUAAACATAATAGCTTCTGTGCGCC -3	55	10	12	8	35
UA2 UA-rich DNA Anti Sense	5'C6amineGGCGCACAGAAGCTATTATGUUUAAUUAUUAUAAAUAAUAUUUUAAUUUAUUAAUUAUUAAUUAUUAAUAUAAUAUAUUUAAUUUAUUAUUAAUAUUAUACTTCTATCAGCATCACCGCT -3'	45	10	8	12	45
CG1 CG-rich DNA	5'AGCGGTGATGCTGATAGAAGCGCGACTGCCCGCCGAGATATCCTGGGGCGCAGCGCGGACGGATGTCCCACGGGGTTGCCGCGCGCGCCGAGCGCTTCGCCATAATAGCTTCTGTGCGCC-3'	19	20	43	38	
mCG1 Methylated C- rich DNA	5'AGCGGTGATGCTGATAGAAGCG•CGTACG•CG•CGAACG•CGTTATCGTCG•CGTACG•CG•CGACG•CGACG•CG•CGATCG•CGAACG•CG•CGTCGTCG•CG•CGACG•CG•CGCATAATAGCTTCTGTGCGCC-3'	21	19	42	38	
TTT Consecutive T	5'AGCGGTGATGCTGATAGAAGAAATTTAAAAAAAATATTAAAAATATAAAAAAAATAATAAAAAAAATATAAAAATTAAAAAAAATTTAAAAAATAATCATAATAGCTTCTGTGCGCC3'	68	29	11	8	
CCC1 Consecutive C1	5'AGCGGTGATGCTGATAGAAGGGCGGGTTAGGCAGGGAGGTGGGCGGGCGGGTGGGGCGGGATGGGCGGGTATGGGCGGGATTGGGCGGGATGGGCGGACATAATAGCTTCTGTGCGCC-3'	17	20	63	17	
CCC2 Consecutive C2	5'-GGCGCACAGAAGCTATTATGTCCGCCCATCCCGCCCAATCCCGCCCATACCCGCCCATCCCGCCCCACCCGCCCGCCCACCTCCCTGCCTAACCCGCCCTCTATCAGCATCACCGCT -3'	20	17	17	63	
TA 100	5'AGCGGTGATGCTGATAGAAGAAATATATTATATTAATAATTAATAATTAATAAATTAAAATATTATTTATAATAATTAAACATAATAGCTTCTGTGCGCC-3'	44	36	12	8	
TA 80	5'AGCGGTGATGCTGATAGAAGTAATAATTAATAAATTAAAATATTATTTATAATAATTAAACATAATAGCTTCTGTGCGCC-3'	33	27	12	8	
TA 60	5'AGCGGTGATGCTGATAGAAGTATTATTTATAATAATTAAACATAATAGCTTCTG TGCGCC-3'	20	20	12	8	

Table 1. A list of DNA sequences used in this research. A yellow or green shading denotes a forward, reverse primer region respectively, under line is CpG methylation; a dot denotes a BstUI restriction site.

2.1.2 Polyamine

To aggregate negative charged dsDNA molecules, positive charged molecules are needed following stoichiometric relation. Previous molecular dynamics (MD) simulation data explained quarter-valent positive charged molecules can attract dsDNAs by bridging between dsDNA molecules unlike mono-valent and di-valent. (Figure 2.4.)

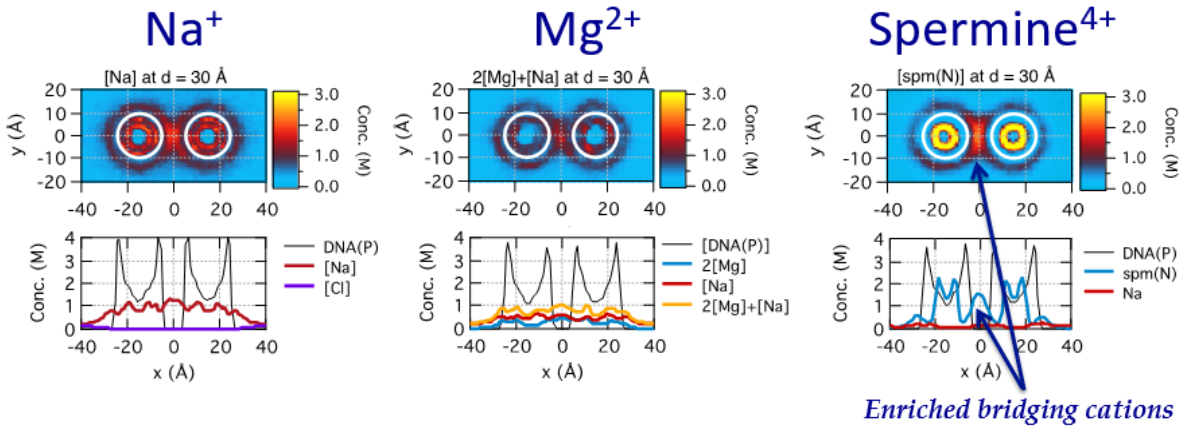

Figure 2.4. Representative distributions of sodium, magnesium and spermine ions at the DNA–DNA distance of 30 Å for the DNA pairs. Spermine ions are densely concentrated between dsDNA backborns compare to sodium, magnesium ion.

Based on this MD simulation data, we selected polyamine molecules, Spermine and Hexa-lysine, to measure methylation dependent dsDNA attraction. (Figure 2.5) In stoichiometric, spermine and Hexa-lysine is quarter and hexa-valent positive charged molecules enough to attract two dsDNAs. In addition, they are structurally linear compare to mono or di-valent ion molecules, they tend to crowd negative charged DNA phosphate backbone side. It acts as bridge, and induce to attract each dsDNA molecules.[12] Biologically, the spermine is known to be a crucial epigenetic factor[43] and hexa-lysine (6Lys) as a simple model for the lysine-rich histone tails which are critical targets of epigenetic modifications

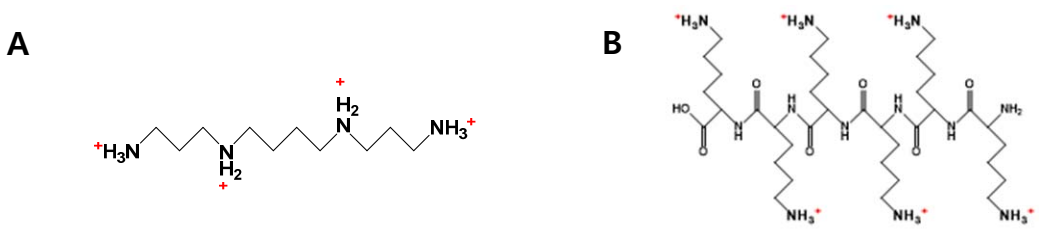

Figure 2.5. Polyamine molecules used in this research (A) quarter-valent positive charged spermine (B) Hexa-valent positive charged lysine (Histone mimic).

2.2 Ensemble FRET Measurement

2.2.1 Spectrofluorometer

Fluorescence spectrophotometers are used to detect fluorophores and quantify their intensity. It have excitation and emission filters to observe the intensity from different fluorophores, so when fluorophore molecules exposed from light of characteristic wavelength in spectrophotometer, they emit photons at a longer characteristic wavelength. From this emission, we can measure emission intensity from each fluorophore molecules. From titration emission intensity, we can measure FRET efficiency.

In this research, Spectrofluorophotometer (RF-5310PC, Shimadzu Scientific Instruments) was used for ensemble FRET measurement. For this experiment, we mixed equimolar (1uM) amount of two kind of the DNA with the same sequence labeled with Cy3 or Cy5 DNA at one end in ensemble FRET buffer (Tris pH8 20mM, EDTA 2mM, NaCl50mM). (Figure 2.6) After then, we measured emission spectrum from 550nm to 700nm using 548 green laser, whenever we injected spermine or 6lysine in original Cy3-Cy5 DNA solution.

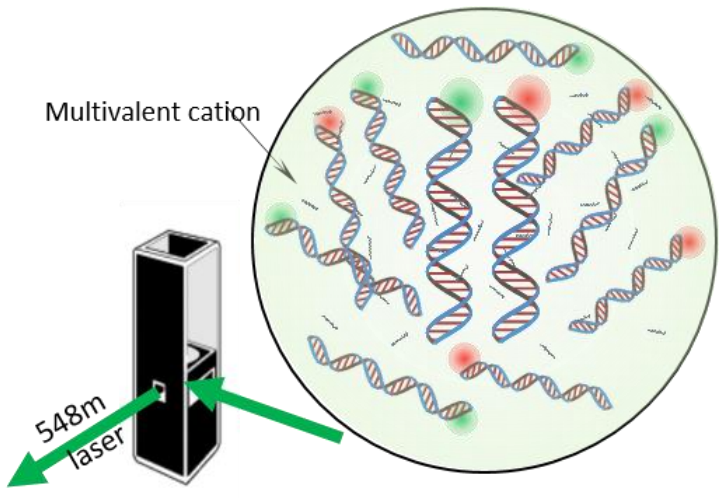

Figure 2.6. Schematic figure of Ensemble FRET. Spectrofluorophotometer cuvette contains equimolar amount of two kinds of the DNA with the same sequence labeled with Cy3 or Cy5 at one end. 548 laser was used for FRET detection. (Methylation dependent 1uM of Cy3DNA, 1uM Cy5 DNA, Tris HCl pH 8 20mM, EDTA 2mM, NaCl 50mM,)

2.2.2 Data Analysis

For ensemble FRET measurement data analysis, we measured energy transfer from donor emission to titrate FRET efficiency. Titration of ensemble FRET data is based on the intensity from 550 to 750 emission spectrum (Figure). Because of difference of quantum yield between donor(Cy3,D) and acceptor(Cy5, A), we decided to use FRET efficiency defined $I=1-I_{DA}/I_{D,}$ where I_{DA} and I_D are the total donor fluorescence intensities in presence and absence of acceptor, respectively. In addition, we have to consider increased 10% volume by adding to spermine or lysine solution, so we revised value by multiplying a reciprocal of increased each volume ratio. For optimal accuracy, fluorescence signal in only buffer solution are eliminated in total solution. All ensemble FRET efficiency was performed for 3times to check the error bars at each polyamine concentrations for each DNA samples. The error bars represent the standard error of mean between these triplicate measurements.

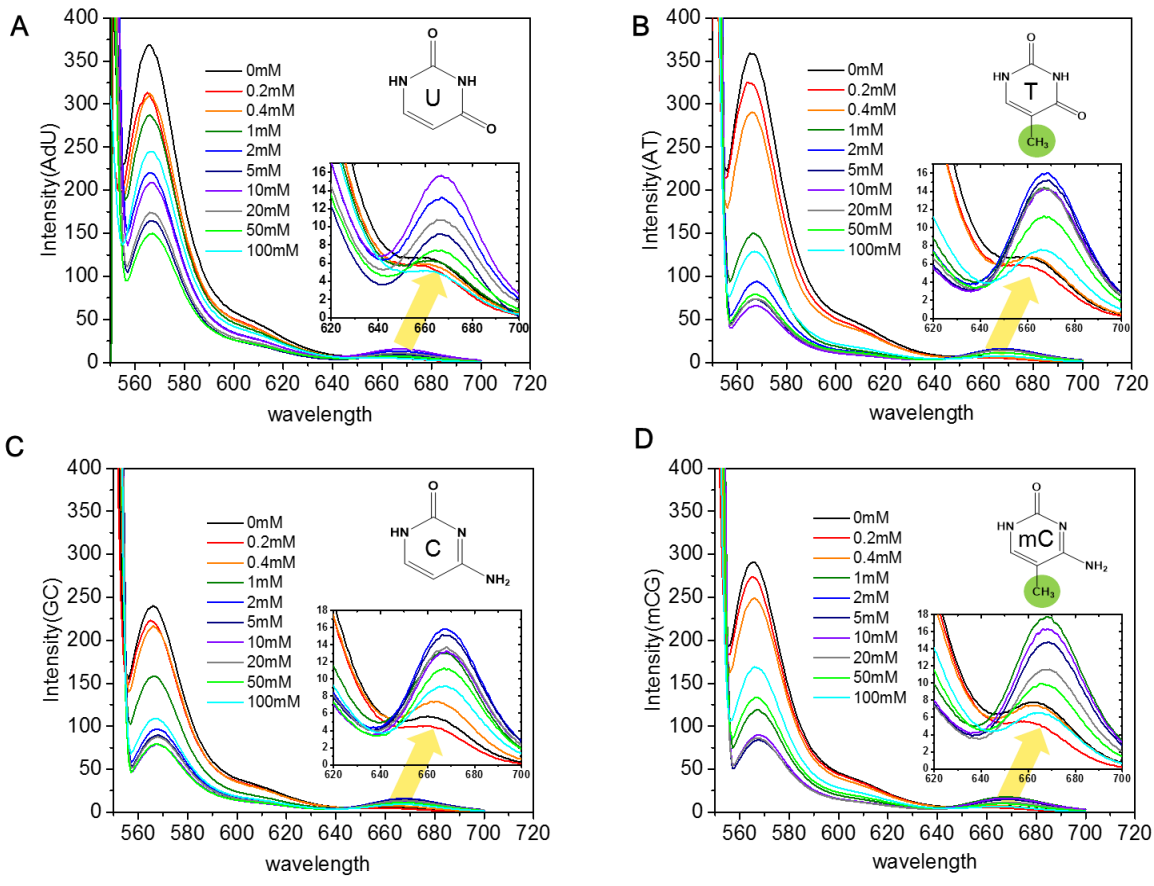

Figure 2.7. Emission spectrum from methylation dependent dsDNA samples in spermine solution. TA and mCG rich DNA (B, C) remarkably decreased in fluorescence intensity of donor (Cy3 550nm) and increased in fluorescence intensity of acceptor (Cy5, 660nm) compare to UA and CG rich DNA (A,C).

2.3 DNA precipitation

Conditions of double-stranded DNA precipitation by the polyamines spermidine and spermine have been determined experimentally and compared to theoretical predictions.[7] We performed DNA precipitation experiment to validate our results more. In our experiment, we presumed that there is difference of supernatant concentration of DNA following strength of DNA condensation governed by methylation. From this supposition, we titrated the concentration of the DNA molecules in the supernatant after precipitating them at varying concentration of the polyamine molecules.

In this experiment, we prepared the 500ml tubes which commonly contain equimolar DNA and precipitation buffer (Tris HCl pH 8 20mM, EDTA 2mM, NaCl 50mM) mixed with each polyamine (spermine/6lysine) in various concentration range from 0mM to 100mM.(Figure 2.8) Then, after 5 minutes incubation in room temperature, centrifuge all concentration range of tubes for 5minute at 14000rpm, and measured the supernatant concentration of each DNA samples using absorb spectroscopy. The concentration of DNA in the supernatant was determined by the measurement of the absorbance at 260nm. All measurement carried out 3times with reproduced DNA and precipitation buffer. We measured from total precipitation solution volume 5ul, 10ul, 20ul, 100ul, and made a difference with incubation or centrifugation time over 10 minutes, there was no difference following the amount of volume and the time range. We normalized the supernatant concentration of each DNA samples. The error bars were determined the standard error of mean between these triplicate measurements.

2.4 Single molecule FRET measurement

2.4.1 Schematic design of multi-color FRET measurement

A recent study showed that the propensity of short dsDNAs to form loops also strongly depends on the methyl content; higher methyl content result in more rigid dsDNAs and higher tendency to unwrap from the nucleosome.[29] In order to reveal the dynamic relation between the DNA-DNA attraction and DNA looping, we performed multi-color single molecule FRET measurements. We labeled one kind of dsDNA with Cy3 and the other with Cy5 and Cy7 at both ends and co-encapsulated them in lipid vesicles (Figure 2.9). Single molecule FRET measurement with alternating excitations of Cy3 and Cy5 allowed us to simultaneously measure the binding (Cy3-Cy5 FRET) and bending (Cy5-Cy7 FRET) dynamics

Because we checked the TA rich DNA has strong condensation compare to other DNA molecules in 1mM spermine, we chose TA rich dsDNA to measure their dynamics at spermine solution with 25mM NaCl.[12] The pair of dsDNA molecules labeled with Cy3, Cy5 Cy7 co-encapsulated with vesicles containing biotinylated lipids in order to immobilize on biotin coated quartz slide.[12](Figure2.9)

To co-encapsulate a pair of DNA molecules, lipid films were made by 1: 100 ratio of 1,2-dipalmitoyl-sn-glycero-3-phosphoethanolamine-N-(Cap-Biotinyl) and dimyristoyl-phosphatidyl-choline (DMPC) (Avanti Polar Lipids, Inc.) and carefully drying with nitrogen gas. The lipids were hydrated with 100uL of buffer solution (100 mM NaCl, and 25 mM TrisHCl, pH 8.0). After hydration, each 1.6 uM of TA rich DNA labeled with Cy3(50μL) and Cy5-Cy7(50μL) was added to the 100uL of buffer solution, to make 400 nM concentration, corresponding to one molecule in a lipid spherical volume of 200 nm diameter, and then the mixed lipid solution was repeatedly frozen in liquid nitrogen and thawed seven times and extruded through 200nm pores of a membrane filter (Whatman, 800281) to make uniformly sized lipid vesicles. By using biotin-neutravidin interaction, the lipid vesicles were attatched on a Polyethylene Glycol-coated surface slide.

Fluorescence signals were measured by EMCCD camera from total internal reflection (TIRF) microscopy. To elongate of the photo bleaching time, we used imaging solution were consist of 1 mg/ml glucose oxidase, 0.04 mg/ml catalase, 0.6% glucose, saturated Trolox (~3 mM), and 25 mM Tris, 25mM NaCl, 1mM spermine. This was optimum condition for checking all mobility between dsDNAs. Fluorescence movies were taken with the rate of 100 millisecond/frame. Green laser of 532 nm and red laser of 647 nm were used as the excitation sources for Cy3 and Cy5 dyes, respectively.

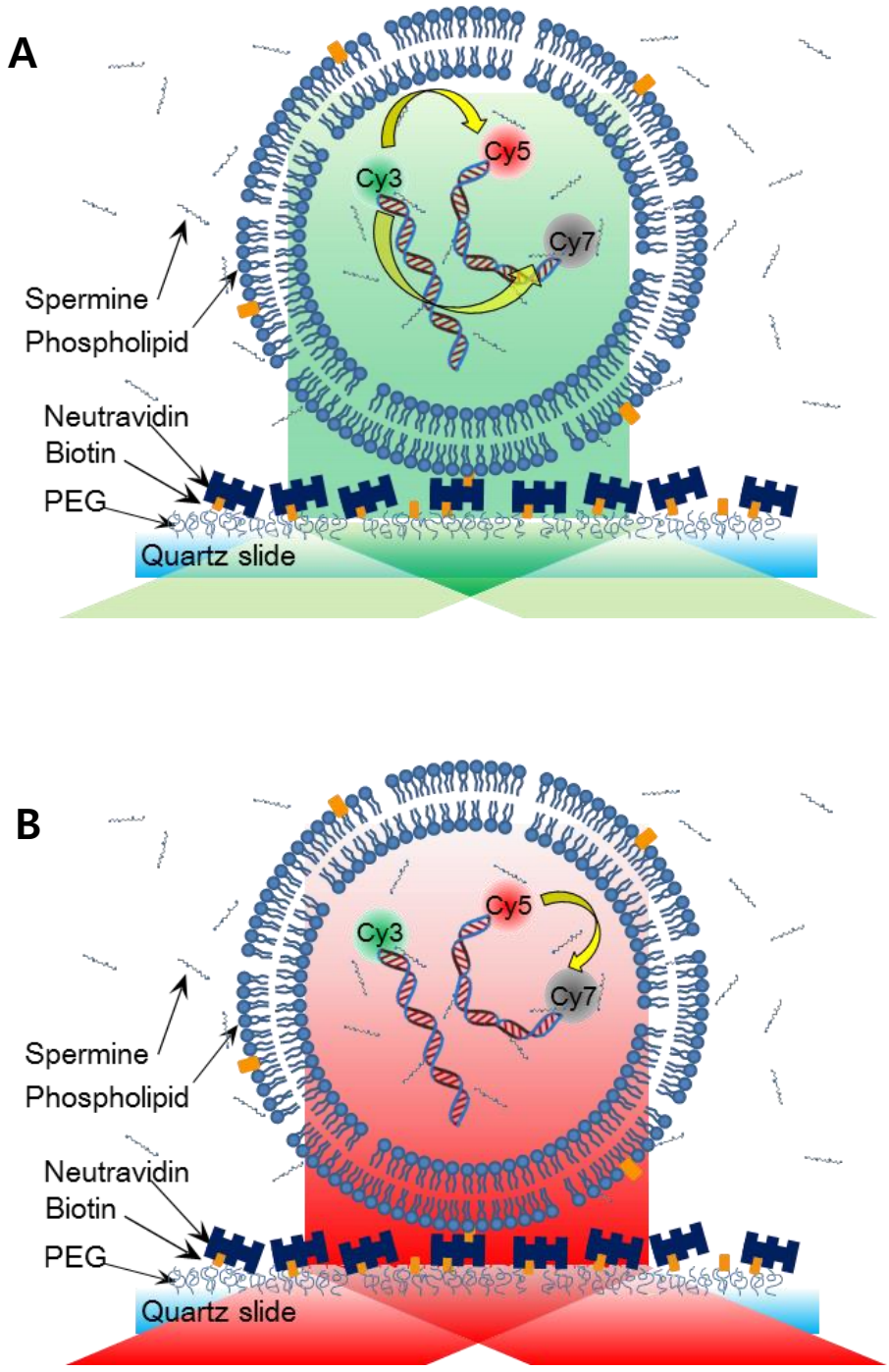

Figure 2.9. Multi-color single molecule measurement using alternate laser excitation. By alternating green and red laser every one hundred milliseconds, we can measure (A) state and (B) state almost at the same time. (A) In the 532nm green excitation state, we can observe the parallel binding events and anti-parallel binding events. (B) In the 647nm red excitation state, we can observe bending events in inter molecular. (100 millisecond/frame, 1mM spermine, 25mM NaCl, 120bp TA rich DNA)

2.4.2 Analysis of single molecule traces

We categorized the diverse FRET events from the fluorescent signals that presented any binding, bending and simultaneous events from selected traces. These traces contain a single pair of donor and acceptor dyes, and all traces were shown heterogeneous dynamics and behaviors. (Figure 2.10)

At first, we picked the traces which were shown single pair of Cy3, Cy5, and Cy7 by checking their signal intensity and bleaching steps from green (532nm) and red laser (647nm) excitation.. To select the traces, we used criteria; when one of three FRET traces (Cy3-Cy5 FRET, Cy3-Cy7 FRET, Cy5 - Cy7 FRET) was shown the FRET signal with other single bleaching steps of fluorescence signal, we chose the traces. The FRET efficiency of over 0.5 was selected from each event or maintaining a FRET level of 0.25. After selected these traces, we categorized each event, parallel binding (Figure 2.10 A), anti-parallel binding events (Figure 2.10 B), bending events (Figure2.10 C), simultaneous events (Figure 2.10 E). Then, we counted each event number from randomly selected 3 single molecule FRET measurement movies, and calculated each trace percentage to predict the dynamics between a pair of dsDNA molecules in 1mM of polyamine.

Based on counted event data, we collected the over 100 of simultaneous events (Figure 2.10 E) to determine cross correlation between bending and binding events. By using cross-correlation, we could measure the behaver similarity of two series: binding, bending, as a function of the displacement of one relative to the other. To exclude the interruption from variable of time difference, we selected simultaneous traces lasted for at least over 30seconds

Furthermore, we drew the scatter plot of FRET population graph which displayed values of averaged FRET levels for binding events and bending events from the 100 of simultaneous event traces. From this scatter plot, we could be able to compare the correlation between binding and bending events when they occur at the same time.

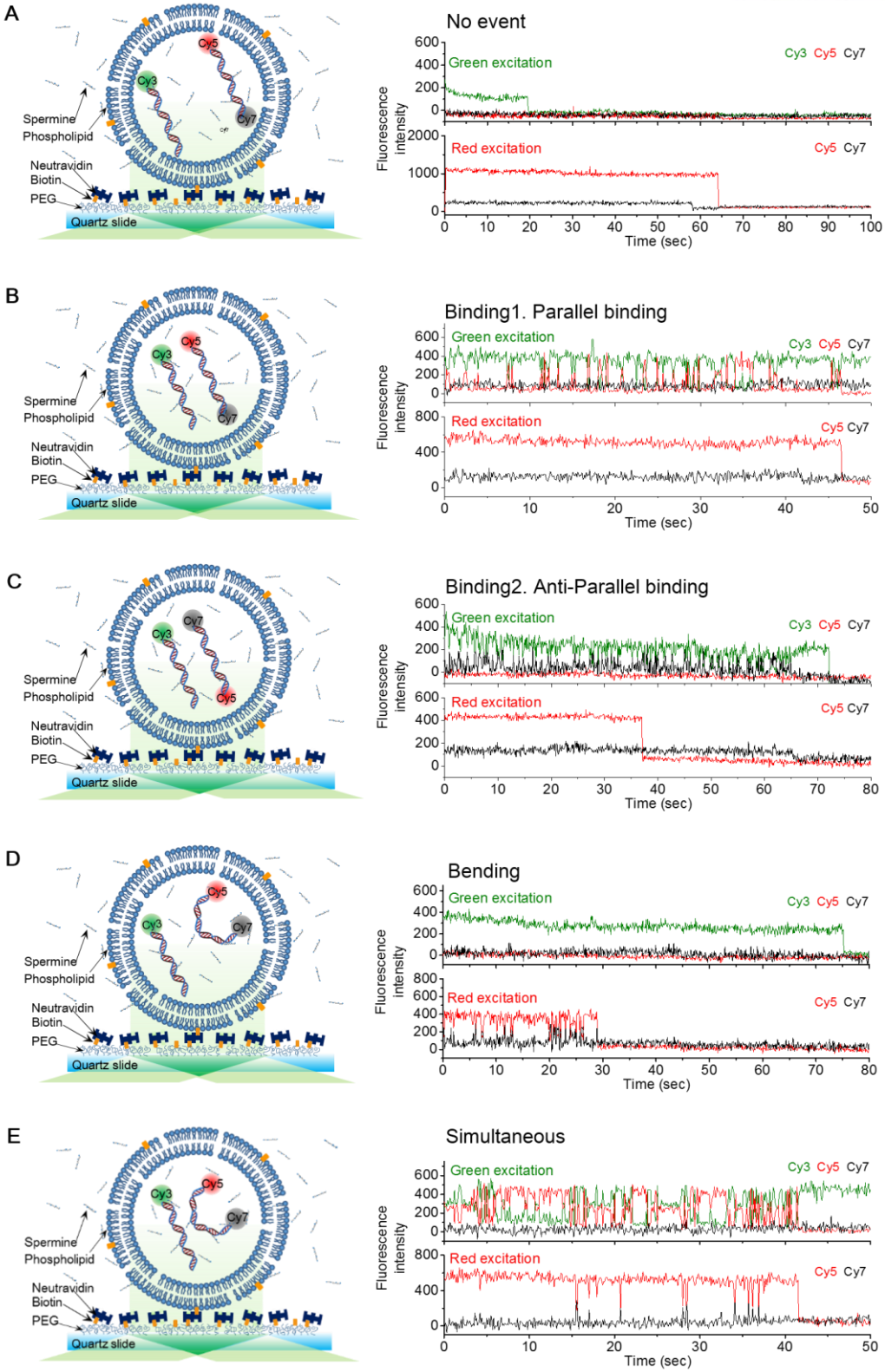

Figure 2.10. Heterogeneous dynamics between dsDNA molecules (A) no event, (B) Parallel Binding event only, (C) Anti-parallel binding event only (D) Bending event only (E) Simultaneous event (Binding & Bending)

Ⅲ. Results

3.1 Ensemble FRET

Through ensemble FRET measurement using spectrometer, we observed the condensation power among each dsDNA group in large volume level by calculating FRET efficiency. In the previous research, TA rich or mCG rich DNA group seems to have many binding frequency than CG rich DNA in the single molecule level[12], so we presumed there is higher affinity between TA or mCG rich dsDNAs than CG rich dsDNA. As we expect, from ensemble FRET measurement, the TA-rich DNAs showed stronger propensity to form aggregates than the CG-rich DNAs as the FRET level rose at 2-3 times lower concentration of spermine or 6Lys (Figure 3.1) Such trend was inverted as we removed the C5 methyl group from the TA-rich DNAs (i.e. UA-rich) or added it to the CG-rich DNAs (i.e. mCG-rich), consistently for both spermine and 6Lys. These results suggest that the content of C5 methyl group, rather than the sequence composition of the DNA, determines the condensation power by linear polyamine molecules. Because there are differences of cation valency and structure between spermine and 6lysine, we could observe stronger condensation in lower concentration of 6lysine6+ compare to spermine4+. Moreover, we also checked the resolubilization point of positively charged DNA-multivalent cation complex in 50mM of spermine4+ or 10mM of Lysine6+ solution. It also reflects valency and structure dependent resolubilization point shift.

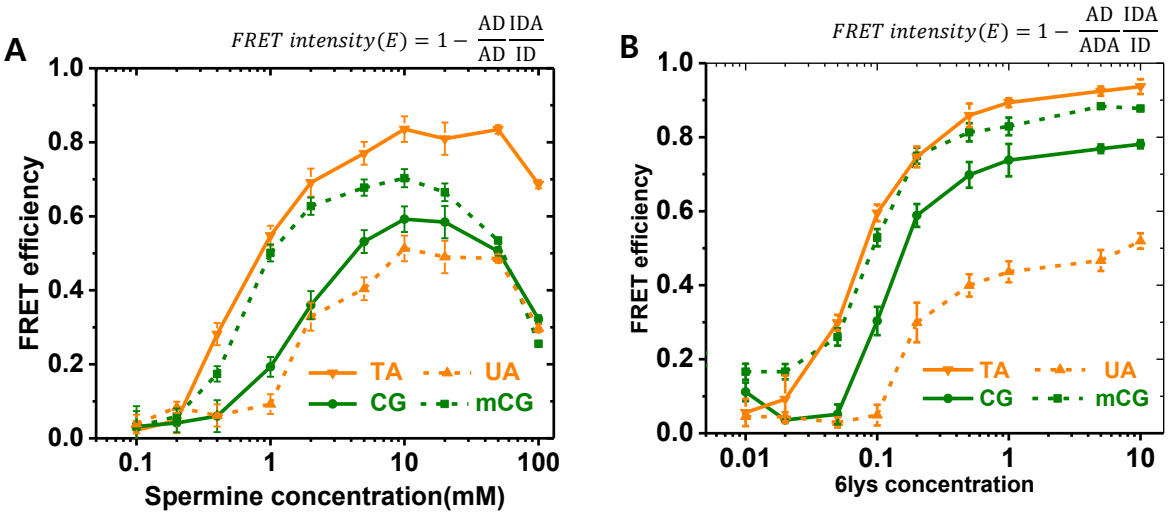

Figure 3.1. Ensemble FRET efficiency titration. (A) Ensemble FRET result using methylation dependent DNA samples in various spermine concentration range. (B) Ensemble FRET result using methylation dependent DNA samples in various 6lysine concentration range

3.2 DNA precipitation

Similar trend between TA and CG-rich DNAs and its inversion by controlling the methyl group were also observed by the precipitation measurement (Figure 3.2). The concentration at which the DNAs start to form aggregates was consistently lower for DNAs containing the methyl group. That transition concentration for spermine was 0.1-1 mM which is close to its physiological concentration [44]. Like ensemble FRET assay, resolubilizations between each dsDNA samples seems to start over 100mM and 10mM in spemrine4+, 6Lysine6+ respectively

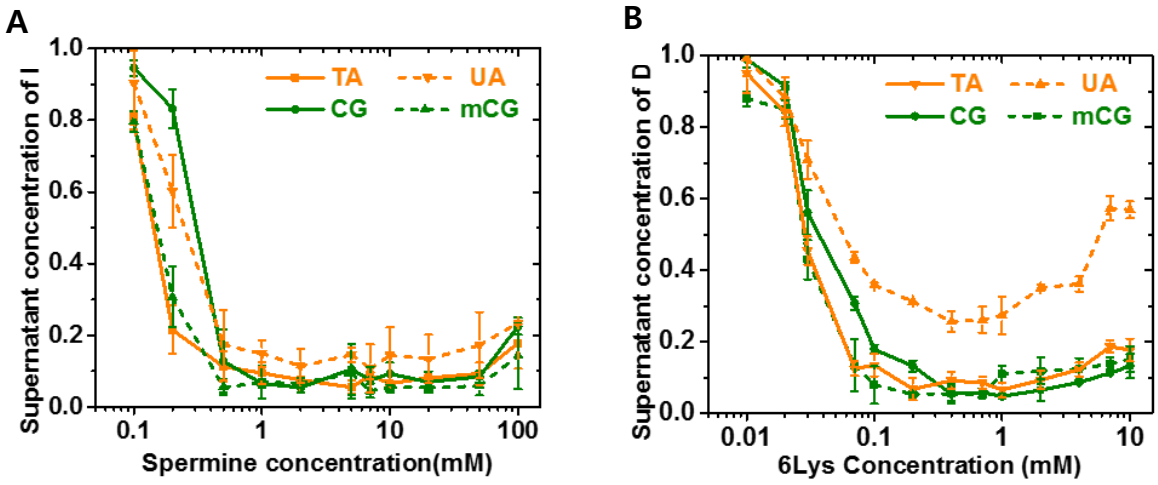

Figure 3.2. Normalized supernatant concentration of DNA using methylation dependent DNA samples after DNA precipitation measurement. (A) DNA precipitation measurement result using methylation dependent DNA samples in various spermine concentration range. (B) DNA precipitation measurement result using methylation dependent samples in various 6lysine concentration range.

Next, we rearranged the DNA sequences keeping the same nucleotide composition so that they have more consecutive sequence motifs (TTT and CCC) to observe consecutive methylation pattern whether effect on DNA condensation power. As we expected, we observed enhanced contrast between them(Figure 3.3), consistent with previous computational prediction.[12] Thus, the effect of the methyl content is maximized when we have the methyl groups consecutively on the same DNA chain, likely due to the linear structure of the polyamine molecules.

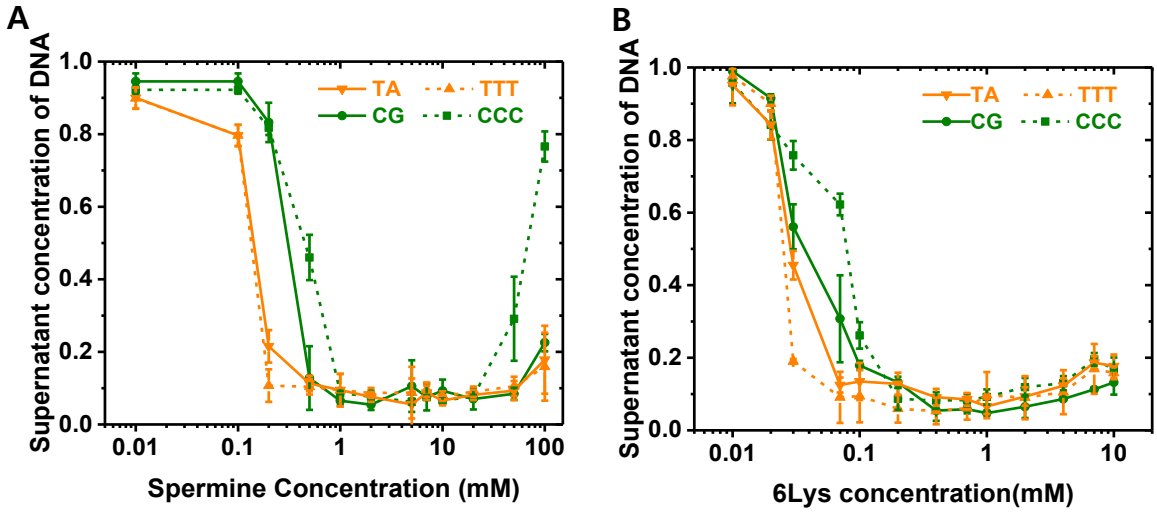

Figure 3.3 Methyl group pattern also affect the condensation power between dsDNA molecules (A) Normalized supernatant concentration of DNA using methyl group pattern dependent samples after DNA precipitation measurement in diverse spermine concentration range (B) in diverse 6lysine concentration range.

Along the same lines, we designed the DNA sequence reducing Thymine number with length to performe the DNA precipitation measurement to observe the propensity of condensation between length dependent dsDNA molecules. The shorter DNA molecules saw a dramatic reduction of the condensation power at polyamine solution.(Figure 3.4.)

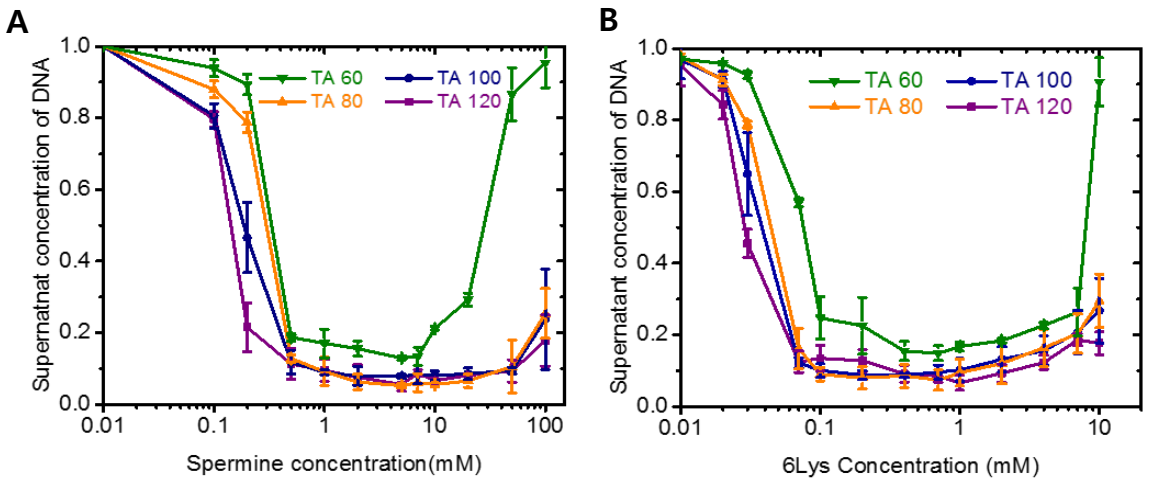

Figure 3.4. Length dependent dsDNA attraction. (A) Normalized supernatant concentration of DNA using Length dependent samples after DNA precipitation measurement in diverse spermine concentration range (B) in diverse 6lysine concentration range

3.3 Multi-color FRET measurement.

By quantifying multi-color FRET measurement results, we could get the statistical number of dynamics between TA rich dsDNA molecules at 1mM spermine solution with 25mM NaCl mono-valent background (Table 2, Table3). Usually, there were about 40% of heterogeneous dynamic events. These 40% of dynamic events were divided into binding (parallel, anti-parallel), bending, and simultaneous events. This statistical data provide some information about dynamics between dsDNA molecules. In the red box on table 2, we could check that parallel binding events occur almost 2~3times more than anti-parallel binding events in the same condition, consistent with previous research[12] Furthermore, we could identify there is anti-correlation between bending and binding events, by comparing the ratio among the binding fraction, bending fraction to level of the TA rich constructs, and their simultaneous events (Figure3.5)

Table 2 : Event count

Movie set	No event (pairs)	Parallel binding events	Anti-parallel binding events	Bending events	Simultaneous events
1	62	12	6	18	2
2	80	16	5	20	1
3	83	13	5	30	2
total	225	57		68	5

Table 3 : Event ratio

Movie set	No event (pairs)	Parallel binding events	Anti-parallel binding events	Bending events	Simultaneous events
1	0.62	0.18		0.18	0.02
2	0.65	0.17		0.16	0.01
3	0.62	0.14		0.22	0.02
average	0.63	0.163		0.19	0.018

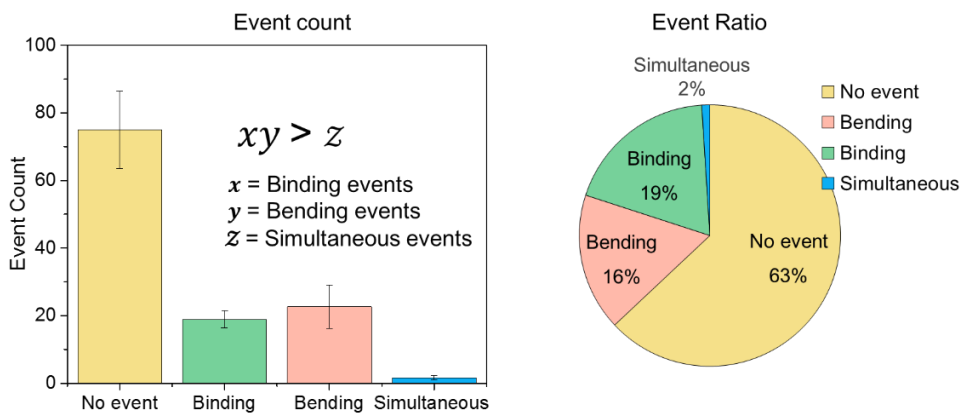

Table 2. , Table3: Count of each events, and Event ratio from multi-color single molecule measurement.

Figure 3.5. The graph from table2 (left) and table3 (right)

To validate this estimation, we collected over the 100 of simultaneous traces lasted for over 30 second, and analyzed the correlation between bending and parallel binding events. Interestingly, these two dynamics were strongly anti-correlated; i.e. when one happened, the chance of the other was significantly reduced (Figure 3.6).

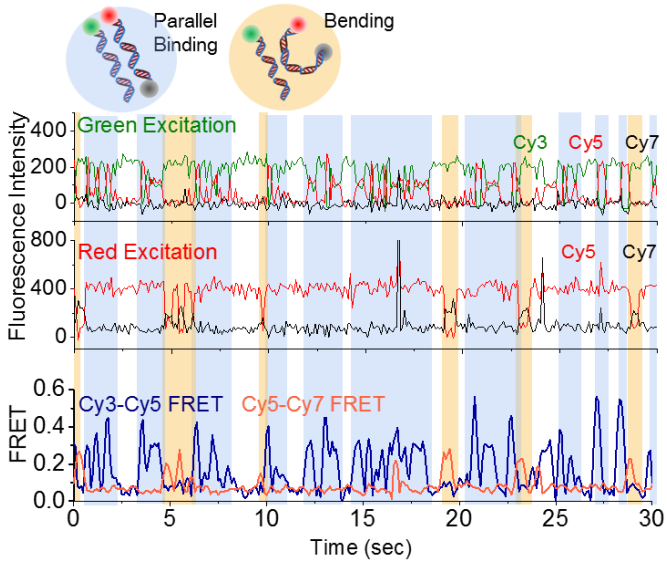

Figure 3.6. Representative simultaneous trace. We can observe anti-correlation between binding event from green excitation (blue shading, trace on the top) and bending event from red excitation (orange shading, trace on the middle), the overlaid FRET trace from Cy3-Cy5 FRET and Cy5-Cy7 FRET(trace on the bottom) clarify the anti-correlation.

For more specific analysis, we computed and plotted a cross correlation between bending and binding events from collected the 100 of simultaneous traces. As we expected, cross-correlation of the two FRET signals exhibited negative correlation over ~ 9 sec, when averaged over 100 single molecule traces selected in unbiased manner (Figure 3.7 A).

Moreover, Scatter plot of the average FRET levels over the individual molecules also revealed the negatively correlated tendency of the two dynamics (Figure). In the Scatter plot of the average FRET from binding and bending events, we could predict when many binding events happen in one simultaneous trace, bending events were rare and vice versa . From that reason, we could not observe simultaneously high FRET frequency and ratio between binding and bending events at the same time. Therefore, we confirmed that binding and bending events between dsDNA molecules are anti-correlated.(Figure 3.7 B)

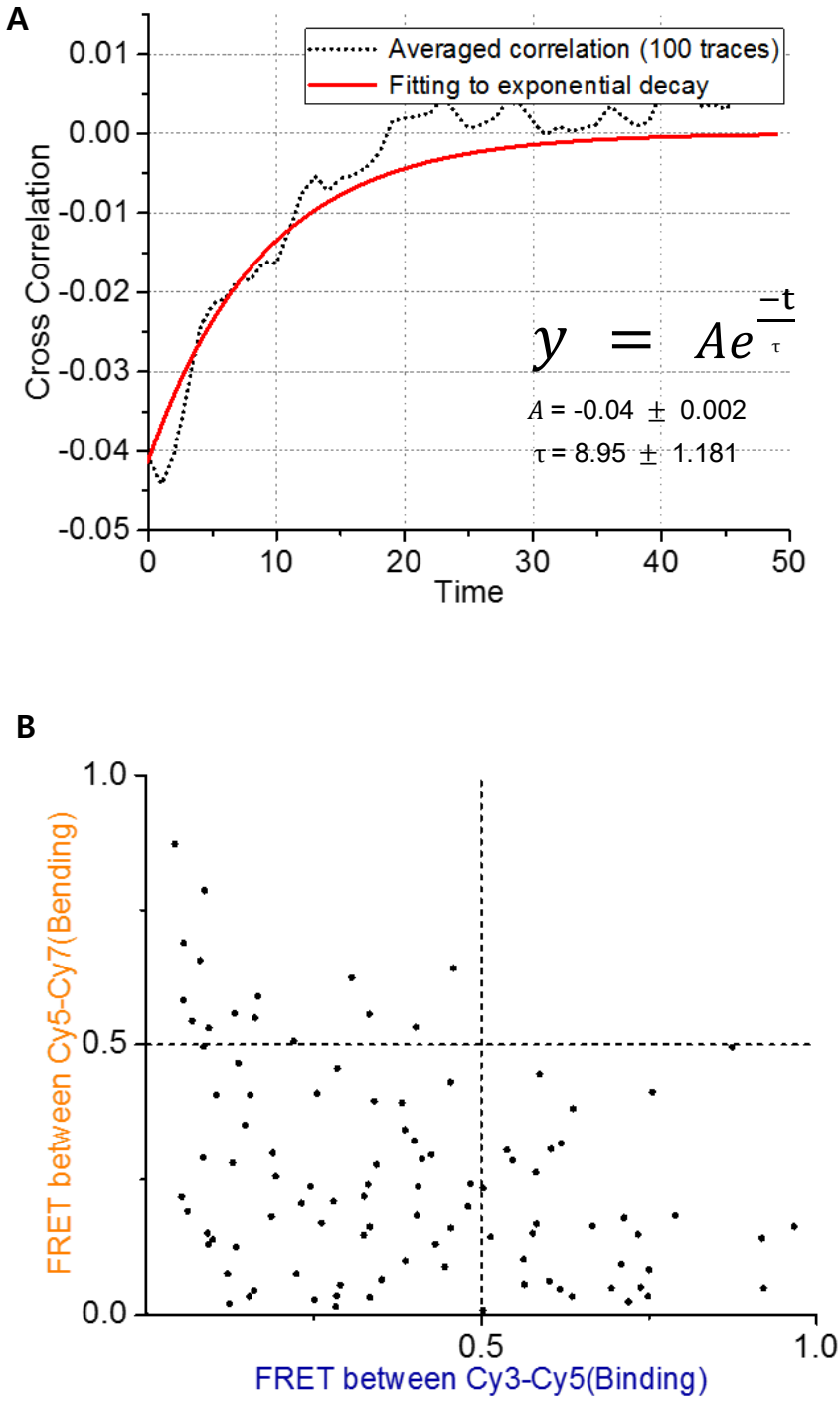

Figure 3.7. Cross correlation graph (A) and Scatter plot (B)

IV. Discussion and Conclusion

4.1 Discussion

In this study, we quantified the polyamine-driven condensation of sequence-controlled and chemically modified DNAs by ensemble FRET and DNA precipitation measurements. Our results are consistent with previous single molecule FRET measurement,[12] and our observations expanded previous studies using spermine with hexa-lysine as histone mimic. We suspect that methyl group on DNA base affects the strength of DNA-DNA attraction regardless of polyamine cation type.

In order to reveal more specific mechanism behind the DNA-DNA attraction with polyamine cation molecules, we performed all-atom molecular dynamics simulations (MD simulation) using our methylation dependent DNA samples. For MD simulation, we designed a simulation box having periodic boundary condition with two parallel dsDNAs (Figure 4.1). Then hexalysine (Lys6+) or spermine molecules and Na+/Cl– ions as well as the explicit water molecules and let the system equilibrate while keeping the dsDNAs at desired distance. We quantified two parameters: the density of the charged elements of polyamines (Lys6+: lysine heavy atom, spermine: nitrogen atom) at the bridging region and the attractive potential energy curve between dsDNAs. The potential energy curve was measured by the umbrella sampling method by fitting the distance population of the ensemble to Boltzmann distribution. At each distance, we averaged the parameters over 100 ns simulation trace.

The number of bridging polyamines were larger for the TA-rich DNAs than CG-rich DNAs at all distances (Figure 4.1 G, I). Remarkably, the potential curves for the methylation-controlled DNAs (UA and mCG) coincided with those for the natural DNAs with the same methyl content, in case of spermine (Figure 4.1 I). Such methylation-dependent polyamine density can be explained by the steric repulsion by the C5 methyl group. The methyl group in TA- and mCG-rich DNAs pushes the bulky polyamine molecules out of the DNA grooves, resulting in lower density of polyamine within the boundary of the double helix (Figure 4.1 C, F). In order to neutralize the phosphate charges, the expelled polyamines are located at the boundary of the DNA (Figure 4.1 C, F, G, I), leading to stronger attraction between dsDNAs. Due to this difference in the charge distribution in the system, TA- or mCG-rich DNAs exhibit larger attractive potential (Figure 4.1 H, J).

This MD simulation results enable us to check that steric repulsion of the polyamine cation molecules by C5 methyl group increases the dsDNA affinity. Based on this physical mechanism for DNA-DNA attraction, we can expand the methylation area into biogenic polyamine molecules. Because steric repulsion is a kind of interaction in a confined space, we can expect that there may be stronger steric repulsion from synergy between DNA methylation and polyamine methylation for dsDNA affinity.

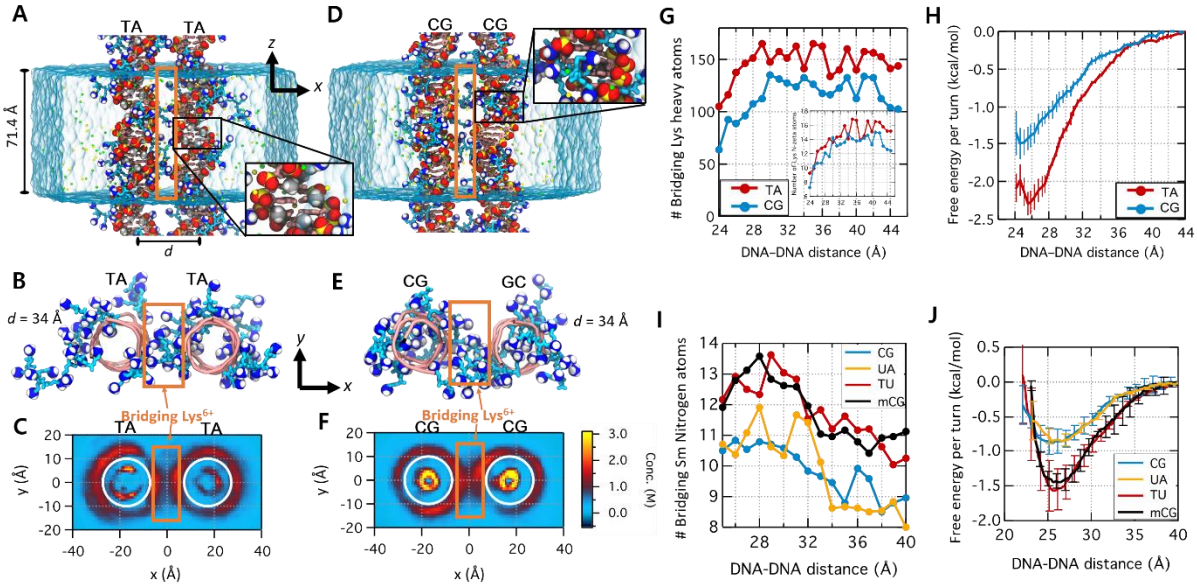

Figure 4.1. Lys6+ -mediated DNA sequence recognition observed in MD simulations. (A) Set-up of MD simulations with a pair of parallel 21-bp TA-rich dsDNAs, (TA)10A·(TA)10T, that are effectively infinite under periodic boundary conditions in an aqueous solution (semi-transparent surface) of 14 Lys6+ molecules (blue) and 100 mM NaCl. Functionally important chemical groups—amine of lysine side chains, phosphate of DNA backbone, and methyl groups of thymine base—are emphasized with spheres colored by atom types: nitrogen, blue; carbon, gray; oxygen, red; phosphorus, yellow; hydrogen, white. For umbrella sampling simulations, d. (inset) A representative conformation of major grooves free from Lys6+ due to steric hindrance of methyl groups. (B) A representative conformation of Lys6+ near TA-rich DNA at d = 34 Å viewed from the top. For clarity, DNA bases are not shown and DNA backbone is shown in pink. (C) The local concentration of Lys6+ N atoms averaged over z axis is shown as a heat map. White circles of 1 nm radius indicate DNA helices. (D–F) are the same plots as panels A–C for the pair of CG-rich dsDNAs, (CG)10G·(CG)10C. (inset) A representative conformation of the major groove filled with Lys6+. (G) The number of bridging Lys6+ heavy atoms (or N atoms in inset) as a function of the DNA–DNA distance. Bridging Lys6+ molecules are the Lys6+ inside the orange boxes shown in panels A–F. (H) Interaction free energy of the two DNA helices as a function of d for two different sequences. (I,J) The same type of analyses done for spermine with pairs of TA-, UA-, CG-, or mCG-rich dsDNA.

There are many polyamine residues such as lysine, arginine on histone H3 tail, It is well known that lysine residue play important role in epigenetic control of heterochromatin assembly.[45] Especially many studies have presented tri-methylated histone H3-K9 and H4-K20 can be found in heterochromatin region[46, 47], and the relation between tri-methylation on histone tail and protein mediated epigenetic regulation[48, 49]. However, from our study about methyl-group effect on DNA condensation, we can presume that not only DNA methylation but also polyamine methylation affect the DNA condensation power from steric repulsion of methyl groups against each other. From this hypothesis about steric repulsion synergy among methyl groups, we performed DNA precipitation to measure condensation power between dsDNAs molecules by using tri-methylated 6lysine and our methyl group dependent DNA samples. (Figure 4.2 A)

In the first measurement, we could see the possibility of methyl group synergy in DNA condensation. Both TA and CG rich DNA with tri-methylated 6lysine settled to the bottom of tube faster at lower concentration than at just 6lysine (Figure 4.2 B, C). From these results, we assumed that the steric repulsion synergy between DNA and polyamine methylation also affects DNA condensation.

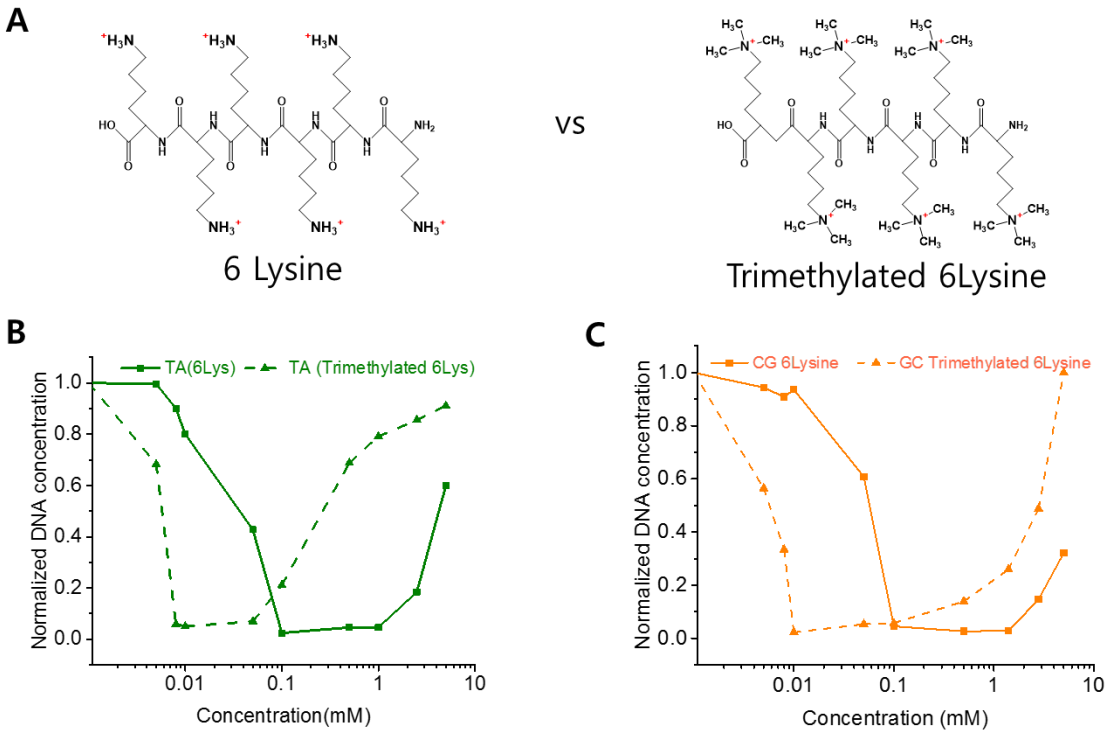

Figure 4.2. (A) Hexa-lysine (6lysine), and Tri-methylated Hexa-lysine as histone tail mimic. They are structurally similar and equally hexa-valent positive charged molecules (B) DNA precipitation result using TA rich DNA at 6lysine and Trimethylated 6lysine. (C) DNA precipitation results using CG rich DNA at 6lysine and Trimethylated 6lysine.

However this measurement had unexpected singularity regarding pH value of buffer solution unlike previous measurements using spermine. When we used the tris buffer pH 8 for pH adjustment of total solution, the precipitation reaction at tri-methylated lysine could not be observed in all concentration range. The synergy from methylated lysine and methyl group on DNA for DNA condensation appeared when we measured after pH adjustment on original lysine solution under pH 6.5 with saline solution. We predict that the DNA condensation difference at tri-methylated lysine according to the pH value may be related with hydrophobic property of methyl group, H+, OH- ion charge effect which also were suggested in recent study about DNA flexibility governed by C5 modifications.[29] These predictions suggest that not only spatial mechanism but also chemical property in single molecule level are important role in dsDNA dynamics such as condensation and flexibility.

Based on this physical mechanism of dsDNA dynamics, we can raise the question whether positive charge pattern and the structure of polyamine cation molecules also control the dsDNA condensation as previous our experiment which presented DNA methylation pattern play a key role in DNA condensation. In order to find the polyamine pattern effect on DNA condensation, we designed new polyamine molecule which alternately arranged with lysine (K) and alanine (A): 6KA (KAKAKAKAKAKA).(Figure 4.3 A) By using this molecule, we performed DNA precipitation measurement like previous experiment to observe the polyamine charge arrangement and structure effect on DNA condensation. As the result, we could observe the different condensation power between dsDNA molecules at 6K or 6KA. Both TA rich and CG rich DNA at 6K precipitated lower concentration than at 6KA. In addition we also observed same tendency of methyl group dependent dsDNA condensation power: TA rich DNA settled to the bottom faster than CG rich DNAs at lower concentration of both 6K and 6KA. (Figure 4.3 B) Because we designed 6K and 6KA as the histone mimic, It may explain the emerging view that different histone tail have different structural roles in chromatin.[50, 51] From this, Positively charged histone tails were suspected to be strongly involved in inducing inter-DNA or inter-nucleosome interaction with previous our methylation dependent dsDNA condensation measurement using 6K. Based on this prediction and the result of polyamine dependent our measurement, we could suspect that diverse physical mechanism from spatial and chemical property of biological molecule highly related with the dsDNA dynamics

Along the same lines, Recent study about DNA looping presented hydrophobicity of C5 methyl group induce the least flexibility compare to other C5 modifications, [29] and MD simulation results from our research suspected that there is steric repulsion from methyl group when TA rich or mCG rich DNA condensate. From these findings, we suspected there is some correlation between DNA flexibility and DNA condensation, and we observed anti-correlation mobility between binding and looping at spermine.

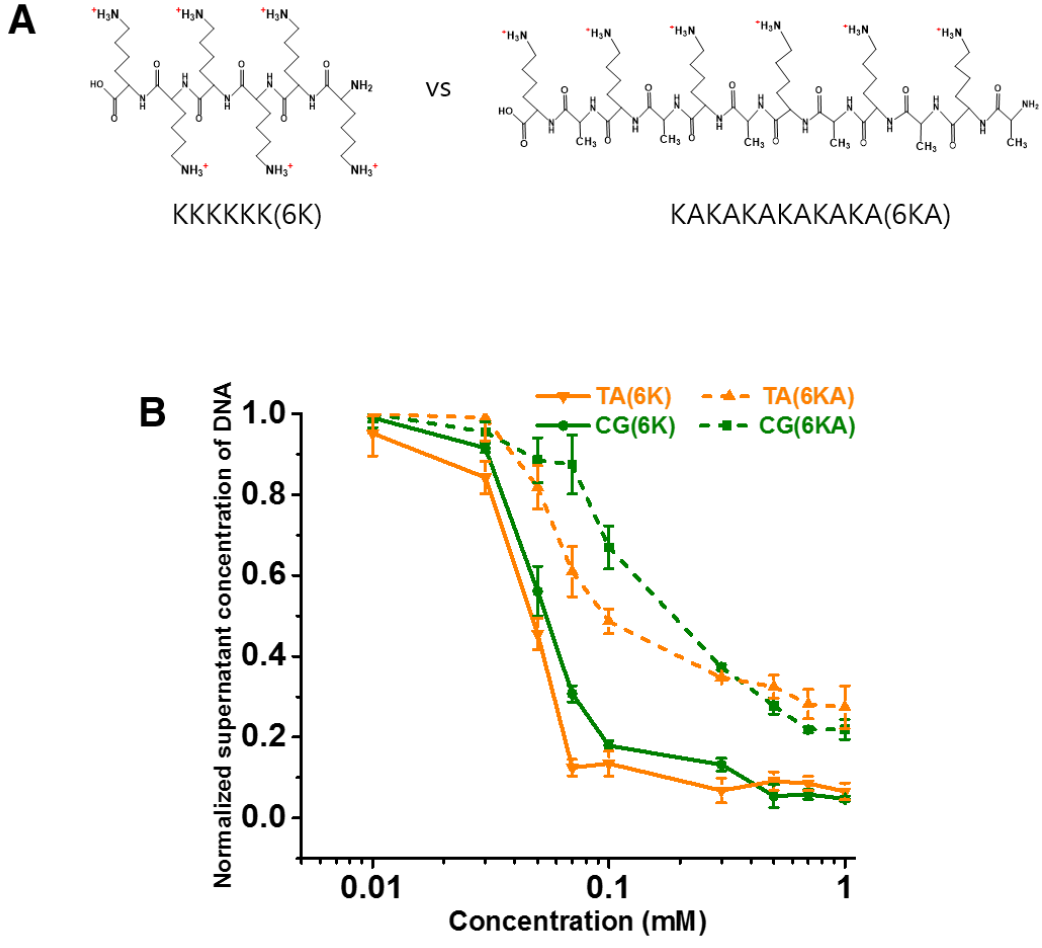

Figure 4.3. Positive charge pattern or structure of polyamine affect DNA condensation. (A) The structure of 6K (Consecutive polyamine molecule), and 6KA (Alternately arranged polyamine molecule with Alanine) (B) DNA precipitation measurement using TA rich and CG rich DNA at 6K and 6KA.

We also performed the multicolor FRET measurement using 6lysine and TA rich DNA to test whether there is the same tendency of anti-correlation, compared to previous spermine measurement. As the result, we could observed obvious anti-correlation between binding and bending event like spermine experiment (Figure 4.4). When binding event happened, significantly reduced bending events were observed (Figure 4.4 A) we could compute obvious negative cross correlation graph using just 10 traces. (Figure 4.4 B)

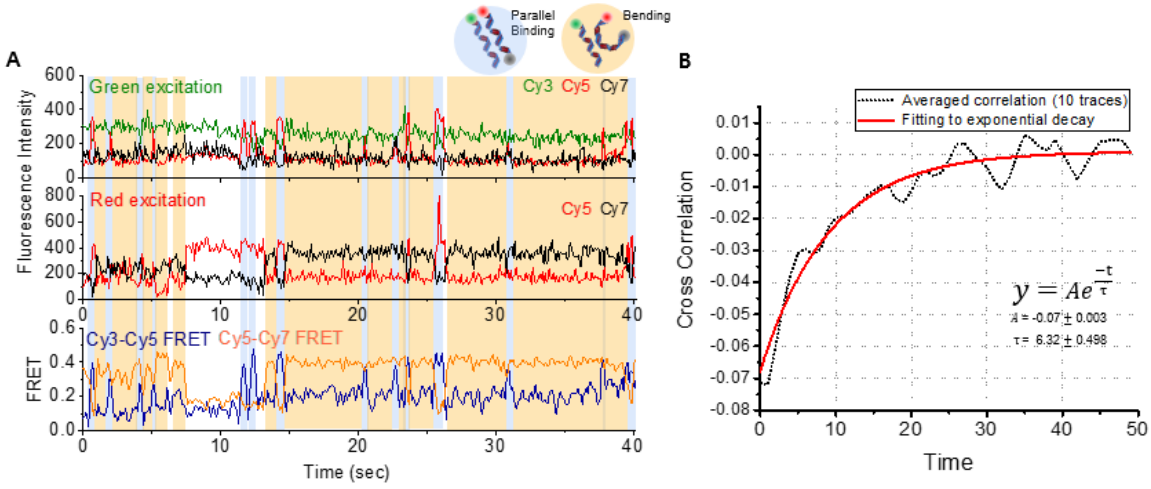

Figure 4.4 Multi color single molecule measurement at 6lysine. (A) Representative single molecule FRET trace from alternate green and red laser excitation and each FRET efficiency. Blue shadings show the binding events and orange shadings show the bending events. (B) Cross correlation graph from 10 of simultaneous traces at 6lysine (120bp TA, 25mM Tris pH 8, 25mM NaCl, 1mM 6lysine)

DNA mobility also important role in gene regulation such as accessibility to binding of transcription factors,[2, 52] , and spatial compartmentalization of chromosomal domains[21] Based on our findings about dsDNA dynamics and current improvement of super-resolution imaging and DNA probe system, we may investigate such large scale inter-segmental interactions at the cellular level.

Recent study showed a new synthetic system that enables cells to record lineage information and event histories in the genome in a format that can be subsequently read out in single cells in situ, by using CRISPR Cas9 system and single molecule Fluorescent in situ hybridization.[53]. By labeling the complete set of loci, we are going to analyze the structural correlation between them and probe the topological arrangement between distant loci, induced by long range affinity between territories. Applying our finding about anti-correlated dynamics between dsDNA molecules with this experiment may potentially reveal the hidden mechanism of large-scale epigenetic changes during cell differentiation or cancer development

4.2 Conclusion

We have found that the C5 methyl group on thymine or methylated cytosine is the key determinant for inter-dsDNA attraction and the inter-dsDNA dynamics is negatively correlated with the looping dynamics. We suspect that these findings have profound implications in epigenetics.

Hyper-methylated chromosomes were found to result in the shutdown of the hyper methylated genes [20] Chromosomal domains were shown to segregate into two compartments depending on their TA content from recent super-resolution imaging. [54] We propose that the methylation-dependent DNA aggregation provides the molecular foundation for the understanding of chromosome organization and epigenetic gene regulation.

In addition, we newly presented another polyamine, 6lysine, effects on methylation dependent DNA condensation as analogue to histone tail. Although 6lysine acted like spermine, 6lysine made complicated results on methylation dependent dsDNA condensation according to modifications such as tri-methylation, alternate arrangement. Because histone tail is rich in lysine, there are many study about lysine residue and its modification on histone which control chromatin structures,[55] Especially, H3K9 is well known for epigenetic marks[56]. Our findings from model peptide lysine may provide the key of uncovered fundamental mechanism on DNA dynamics in chromosome organization.

Lastly, we observed anti-correlated movement between binding and bending from a pair of dsDNA. Based on our MD simulation study, we assumed that there is steric repulsion governed by methyl group against polyamine molecule when a pair of dsDNA condensate, and previous study suggested that the hydrophobic property of methylation controls the DNA flexibility such as bending on dsDNA.[29] Because their interests between DNA condensation and flexibility were mutually incompatible, they seem to be anti-correlated in this research.

From this research, we suspect that these complicated physical mechanisms in nature may highly related with fundamental dynamics of a pair of dsDNA molecules, and such behavior may work as the epigenetic gene regulation mechanisms.

Reference

1. Misteli, T., *Beyond the Sequence: Cellular Organization of Genome Function.* Cell, 2007. **128**(4): p. 787-800.
2. Dion, V. and S.M. Gasser, *Chromatin movement in the maintenance of genome stability.* Cell, 2013. **152**(6): p. 1355-1364.
3. Spector, D.L., *The Dynamics of Chromosome Organization and Gene Regulation.* Annual Review of Biochemistry, 2003. **72**(1): p. 573-608.
4. Grewal, S.I.S. and D. Moazed, *Heterochromatin and Epigenetic Control of Gene Expression.* Science, 2003. **301**(5634): p. 798-802.
5. Leng, M. and G. Felsenfeld, *The preferential interactions of polylysine and polyarginine with specific base sequences in DNA.* Proceedings of the National Academy of Sciences, 1966. **56**(4): p. 1325-1332.
6. Hoopes, B.C. and W.R. McClure, *Studies on the selectivity of DNA precipitation by spermine.* Nucleic Acids Research, 1981. **9**(20): p. 5493-5504.
7. Raspaud, E., et al., *Precipitation of DNA by polyamines: a polyelectrolyte behavior.* Biophysical journal, 1998. **74**(1): p. 381-393.
8. DeRouchey, J., B. Hoover, and D.C. Rau, *A comparison of DNA compaction by arginine and lysine peptides: a physical basis for arginine rich protamines.* Biochemistry, 2013. **52**(17): p. 3000-3009.
9. Besteman, K., K. Van Eijk, and S. Lemay, *Charge inversion accompanies DNA condensation by multivalent ions.* Nature Physics, 2007. **3**(9): p. 641-644.
10. Lipfert, J., et al., *Understanding Nucleic Acid–Ion Interactions.* Annual review of biochemistry, 2014. **83**: p. 813-841.
11. Deng, H., et al., *Structural basis of polyamine–DNA recognition: spermidine and spermine interactions with genomic B-DNAs of different GC content probed by Raman spectroscopy.* Nucleic acids research, 2000. **28**(17): p. 3379-3385.
12. Yoo, J., et al., *Direct evidence for sequence-dependent attraction between double-stranded DNA controlled by methylation.* Nature communications, 2016. **7**.
13. Nathan, D. and D.M. Crothers, *Bending and flexibility of methylated and unmethylated EcoRI DNA1.* Journal of Molecular Biology, 2002. **316**(1): p. 7-17.
14. Pérez, A., et al., *Impact of Methylation on the Physical Properties of DNA.* Biophysical Journal, 2012. **102**(9): p. 2140-2148.
15. Ngo, T.T.M., et al., *Effects of cytosine modifications on DNA flexibility and nucleosome*

mechanical stability. Nature Communications, 2016. **7**: p. 10813.

16. Holliday, R., *Epigenetics: a historical overview.* Epigenetics, 2006. **1**(2): p. 76-80.
17. Egger, G., et al., *Epigenetics in human disease and prospects for epigenetic therapy.* Nature, 2004. **429**(6990): p. 457-463.
18. Baylin, S.B., *DNA methylation and gene silencing in cancer.* Nature Clinical Practice Oncology, 2005. **2**(S1): p. S4-S4.
19. Allis, C.D., T. Jenuwein, and D. Reinberg, *Epigenetics*. 2007, Cold Spring Harbor, N.Y.: Cold Spring Harbor Laboratory Press. x, 502 p.
20. Cremer, T. and C. Cremer, *Chromosome territories, nuclear architecture and gene regulation in mammalian cells.* Nature reviews genetics, 2001. **2**(4): p. 292-301.
21. Wang, S., et al., *Spatial organization of chromatin domains and compartments in single chromosomes.* Science, 2016. **353**(6299): p. 598-602.
22. Greer, E.L. and Y. Shi, *Histone methylation: a dynamic mark in health, disease and inheritance.* Nature Reviews Genetics, 2012. **13**(5): p. 343-357.
23. Esteller, M., *DNA methylation, epigenetics, and metastasis*. Cancer metastasis. 2005, Dordrecht ; New York: Springer. xi, 310 p.
24. Lister, R., et al., *Human DNA methylomes at base resolution show widespread epigenomic differences.* nature, 2009. **462**(7271): p. 315-322.
25. Ngo, T.T., et al., *Asymmetric unwrapping of nucleosomes under tension directed by DNA local flexibility.* Cell, 2015. **160**(6): p. 1135-1144.
26. Choy, J.S., et al., *DNA methylation increases nucleosome compaction and rigidity.* Journal of the American Chemical Society, 2010. **132**(6): p. 1782-1783.
27. Rountree, M.R. and E.U. Selker, *DNA methylation inhibits elongation but not initiation of transcription in Neurospora crassa.* Genes & development, 1997. **11**(18): p. 2383-2395.
28. Phillips, T., *The role of methylation in gene expression.* Nature Education, 2008. **1**(1): p. 116.
29. Ngo, T.T., et al., *Effects of cytosine modifications on DNA flexibility and nucleosome mechanical stability.* Nat Commun, 2016. **7**: p. 10813.
30. Cario, G. and J. Franck, *Über zerlegung von wasserstoffmolekülen durch angeregte quecksilberatome.* Zeitschrift für Physik A Hadrons and Nuclei, 1922. **11**(1): p. 161-166.
31. Perrin, J., *Fluorescence et induction moleculaire par resonance.* CR Hebd. Seances Acad. Sci, 1927. **184**: p. 1097-1100.
32. Förster, T., *Zwischenmolekulare Energiewanderung und Fluoreszenz.* Annalen der Physik, 1948. **437**: p. 55-75.
33. Tinoco, I. and R.L. Gonzalez, *Biological mechanisms, one molecule at a time.* Genes &

development, 2011. **25**(12): p. 1205-1231.

34. Ha, T., et al., *Probing the interaction between two single molecules: fluorescence resonance energy transfer between a single donor and a single acceptor.* Proceedings of the National Academy of Sciences, 1996. **93**(13): p. 6264-6268.
35. Hohng, S., C. Joo, and T. Ha, *Single-molecule three-color FRET.* Biophysical journal, 2004. **87**(2): p. 1328-1337.
36. Aitken, C.E., R.A. Marshall, and J.D. Puglisi, *An oxygen scavenging system for improvement of dye stability in single-molecule fluorescence experiments.* Biophysical journal, 2008. **94**(5): p. 1826-1835.
37. Lee, S., J. Lee, and S. Hohng, *Single-molecule three-color FRET with both negligible spectral overlap and long observation time.* PloS one, 2010. **5**(8): p. e12270.
38. Hohng, S., et al., *Maximizing information content of single-molecule FRET experiments: multi-color FRET and FRET combined with force or torque.* Chemical Society reviews, 2014. **43**(4): p. 1007.
39. Baumann, C.G., et al., *Ionic effects on the elasticity of single DNA molecules.* Proceedings of the National Academy of Sciences, 1997. **94**(12): p. 6185-6190.
40. Bloomfield, V.A., *DNA condensation by multivalent cations.*
41. Xu, Y. and H. Sugiyama, *Formation of the G-quadruplex and i-motif structures in retinoblastoma susceptibility genes (Rb).* Nucleic acids research, 2006. **34**(3): p. 949-954.
42. Kim, S.E., et al., *Destabilization of i-motif by submolar concentrations of a monovalent cation.* The Journal of Physical Chemistry B, 2014. **118**(18): p. 4753-4760.
43. Fiori, L.M. and G. Turecki, *Epigenetic regulation of spermidine/spermine N 1-acetyltransferase (SAT1) in Suicide.* Journal of psychiatric research, 2011. **45**(9): p. 1229-1235.
44. SHIM, H. and A.H. FAIRLAMB, *Levels of polyamines, glutathione and glutathione-spermidine conjugates during growth of the insect trypanosomatid Crithidia fasciculata.* Microbiology, 1988. **134**(3): p. 807-817.
45. Nakayama, J., et al., *Role of histone H3 lysine 9 methylation in epigenetic control of heterochromatin assembly.* Science, 2001. **292**(5514): p. 110-113.
46. Martin, C. and Y. Zhang, *The diverse functions of histone lysine methylation.* Nature reviews. Molecular cell biology, 2005. **6**(11): p. 838.
47. Schotta, G., et al., *A silencing pathway to induce H3-K9 and H4-K20 trimethylation at constitutive heterochromatin.* Genes & Development, 2004. **18**(11): p. 1251.
48. Paul, B., et al., *Heterochromatin and tri-methylated lysine 20 of histone H4 in animals.* Journal of cell science, 2004(117): p. 2491.

49. van der Heijden, G., et al., *Asymmetry in histone H3 variants and lysine methylation between paternal and maternal chromatin of the early mouse zygote.* Mechanisms of development, 2005. **122**(9): p. 1008.

50. Hansen, J.C., *CONFORMATIONAL DYNAMICS OF THE CHROMATIN FIBER IN SOLUTION: Determinants, Mechanisms, and Functions.* 2002.

51. Kan, P.-Y., T.L. Caterino, and J.J. Hayes, *The H4 Tail Domain Participates in Intra-and Internucleosome Interactions with Protein and DNA during Folding and Oligomerization of Nucleosome Arrays.* Molecular and Cellular Biology, 2009. **29**(2): p. 538.

52. Brackley, C.A., et al., *Simulated binding of transcription factors to active and inactive regions folds human chromosomes into loops, rosettes and topological domains.* Nucleic acids research, 2016. **44**(8): p. 3503-3512.

53. Frieda, K.L., et al., *Synthetic recording and in situ readout of lineage information in single cells.* Nature, 2016.

54. Boettiger, A.N., et al., *Super-resolution imaging reveals distinct chromatin folding for different epigenetic states.* Nature, 2016. **529**(7586): p. 418-422.

55. Shogren-Knaak, M., et al., *Histone H4-K16 acetylation controls chromatin structure and protein interactions.* Science, 2006. **311**(5762): p. 844-847.

56. Johnson, L.M., X. Cao, and S.E. Jacobsen, *Interplay between two epigenetic marks: DNA methylation and histone H3 lysine 9 methylation.* Current Biology, 2002. **12**(16): p. 1360-1367.